REVIEW

National Science Open
2: 20230002, 2023
https://doi.org/10.1360/nso/20230002

Materials Science

Special Topic: Two-dimensional Materials and Devices

Spin-phonon coupling in two-dimensional magnetic materials

Lili Hu[1], Ke-zhao Du[2], Yuzhong Chen[1], Yuxin Zhai[3], Xingzhi Wang[4,*] & Qihua Xiong[3,1,5,6,*]

[1]*Beijing Academy of Quantum Information Sciences, Beijing 100193, China;*
[2]*College of Chemistry and Materials Science, Fujian Provincial Key Laboratory of Advanced Materials Oriented Chemical Engineering, Fujian Normal University, Fuzhou 350007, China;*
[3]*State Key Laboratory of Low-Dimensional Quantum Physics and Department of Physics, Tsinghua University, Beijing 100084, China;*
[4]*Department of Physics, Xiamen University, Xiamen 361005, China;*
[5]*Frontier Science Center for Quantum Information, Beijing 100084, China;*
[6]*Collaborative Innovation Center of Quantum Matter, Beijing 100084, China*

*Corresponding authors (emails: qihua_xiong@tsinghua.edu.cn (Qihua Xiong); xzwang@xmu.edu.cn (Xingzhi Wang))

Received 10 January 2023; Revised 7 February 2023; Accepted 16 February 2023; Published online 21 June 2023

Abstract: Recently, two-dimensional magnetic materials (2DMMs) have become a focused research direction in a broad range of two-dimensional materials, due to their underlying significance in fundamental research, as well as in technologically relevant applications for future spintronics, magnonics, quantum information and data storage. The rich toolbox of 2DMMs and their diverse tunability have enabled the unprecedented research concerning the two-dimensional magnetic order down to single atomic layer of materials, much beyond the classical thin film magnetism, showing an extremely promising avenue towards electronics, magneto-optics and photonics. Among various degrees of freedoms, the interaction between spin and phonon (i.e., quanta of lattice vibration), hence the so-called spin-phonon coupling, serves as an important tuning knob to explore the two-dimensional magnetism, creates new types of quasiparticles and controls the magnetic order. This review overviews the latest developments in spin-phonon coupling investigations in 2DMMs. Various techniques utilizing spin-phonon coupling to investigate two-dimensional magnetism are discussed. Recent progress in tuning two-dimensional magnetic order based on spin-phonon coupling is also summarized, with a focus to understand the new functionalities. Furthermore, device developments and concepts based on spin-phonon coupling are briefly discussed. This review will provide our perspectives on the existing challenges and future directions in spin-phonon coupling research in 2DMMs and their functional devices.

Keywords: spin, phonons, couplings, dimensional, magnetic, materials

Introduction

Recent breakthroughs in realizing true two-dimensional magnetic materials (2DMMs) sparked renewed interest for the next-generation spintronics [1], magnonics [2], and quantum information technology [3,4]. 2DMMs have shown intriguing properties in spin tunneling junctions [5], spin valves [6], topological superconductivity [7], etc. Among various degree of freedoms and their interactions, spin-phonon coupling is one of the most important interactions that correlate the charge, spin and lattice vibrations, extensively

investigated in prior literature in traditional three-dimensional (3D) multiferroics [8,9]. Strong spin-phonon coupling is also found ubiquitous in 2DMMs, including transition metal halides [10,11], transition metal phosphorous tri-chalcogenides [12,13], ternary iron-based tellurides [14], transition metal oxyhalides [15], and transition metal dichalcogenides [16].

From the perspective of fundamental investigations, spin-phonon coupling can stabilize two-dimensional (2D) long-range magnetic order [17] and modulate the symmetry of materials [18], leading to the emergence of novel phenomena or quasiparticles [19]. In addition, the stretching or deformation of 2DMMs can modify the spin-related mechanical, electrical and optical properties through spin-phonon coupling [20,21]. In terms of applications, spin-phonon coupling attributes 2DMM-based spintronic devices a rich tuning knob flexibility, such as manipulation of magnetic order, propagation of spin waves and transport of spin currents. In particular, through spin-phonon coupling high-speed spintronic or magnonic devices based on 2DMMs can be realized. For example, fast antiferromagnetic spintronic devices can be developed by phonon excitations triggered by THz lights, benefited from the zero stray fields of antiferromagnets [22]. Spin-phonon coupling is also one of the main mechanisms of qubit decoherence [23]. Therefore, controlling the spin-phonon coupling can potentially improve the lifetime of qubits. Moreover, based on the spin-phonon coupling, spintronic devices utilizing the spin Seeback effect can also be developed [17,24].

Spin-phonon coupling can be used as an effective tool to identify 2D magnetism. The Mermin-Wagner theorem states that the long-range 2D magnetism does not exist in isotropic Heisenberg magnets [25]. Later the experimental discovery of intrinsic 2DMMs verified the existence of long-range magnetic order in two dimensions and clarified the applicable conditions of Mermin-Wagner theorem [26,27]. Since the characterization methods of thin-layer magnets, especially monolayer magnets, are quite limited [28], the application of spin-phonon coupling effect plays an important role in verifying atomic-thick 2DMMs, especially monolayers. In addition, compared with magneto-optical Kerr effect (MOKE), magnetic circular dichroism (MCD) and other methods that only detect the magnetic order based on the net magnetic moment of materials, spin-phonon coupling based methods do not have such constraint and thus offer more advantages, which is applicable in antiferromagnets and other novel magnetic materials with or without net magnetic moment. For example, before $Cr_2Ge_2Te_6$ was confirmed to be a 2DMM, its phonon behavior was reported to exhibit an anomalous variation near the Curie temperature (T_C) by Raman spectroscopy [29]. Besides that, the spin-phonon coupling effect led to the discovery of 2D antiferromagnetism in monolayer $FePS_3$ [12,30]. It has been found in 2D itinerant ferromagnetic Fe_3GeTe_2 the magnetic order significantly enhances the frequency softening and intensity of certain phonon modes [31]. In magnetic material VI_3, 2D magnetism was characterized by the circularly polarized Raman intensity of phonons [32]. In $CrBr_3$, the phonon frequency and intensity anomalies due to spin-phonon coupling were identified [33]. Later the spin-phonon coupling induced negative thermal expansion was also discovered in $CrBr_3$ [34].

In addition to verifying the 2D magnetic order in atomically thin layers, the spin-phonon coupling is also investigated systematically as an important coupling mechanism and utilized to manipulate the magnetic properties in 2DMMs. Researchers found that the interlayer interaction in bilayer CrI_3 can regulate the exchange correlation through the spin-lattice coupling, thereby determining the interlayer magnetism of bilayer CrI_3 [10]. Furthermore, the spin-phonon coupling in 2DMMs exemplifies the frequency or intensity anomaly of phonons, such as the cases in CrSBr [35] and CrOCl [36]. Moreover, the arrangement of spins can induce the change of Raman selection rules in certain materials [18,32]. The presence of magnetic order

activates or suppresses the Raman activity of the phonon mode by modifying the parity, showing spin-phonon coupling effect. The hybridization of phonons and magnons will lead to the formation of quasi-particles with novel topological properties [16,19], which may affect the thermal conductivity and other properties of materials. In novel 2D Kitaev quantum spin liquid materials α-$RuCl_3$, the spin-phonon coupling regulates the thermal conductivity, which increases by two orders of magnitude under high magnetic fields [37]. Another case that the intriguing physical phenomenon originating from the spin-phonon coupling was reported in $MnBi_2Te_4$. A_{1g} mode phonons in this material strongly modulate the interaction of interlayer exchange, which is an important reason leading to the appearance of its topological insulating phase [38]. The control of lattice degree was also utilized to reveal different interlayer magnetic orders in $CrBr_3$ [39]. Lately, the application of strain to 2DMMs can greatly modify the magnetic order. It has been demonstrated that the strain can be used to enhance the ferromagnetism in monolayer Fe_3GeTe_2, and control Néel vector in $MnPSe_3$ [14,40]. In CrSBr, a reversible magnetic phase transition has been realized by applying the strain [21]. As shown in Figure 1, developing from a tool for unveiling the 2D magnetism to a route of modifying the magnetic properties, the exploiting of spin-phonon coupling effect shows great potential in spintronics and magnonics.

For this rapidly developing field, we believe that it is timely and pressing to overview the latest development in the spin-phonon coupling in the large family of 2DMMs. We organize this comprehensive review in the following layout. Firstly, we will summarize the latest developments of spin-phonon coupling in several typical 2DMMs and the relevant theoretical investigations; secondly, we will review various techniques utilizing spin-phonon coupling to investigate the two-dimensional magnetism; thirdly, we will highlight several experimental approaches in tuning two-dimensional magnetism based on spin-phonon

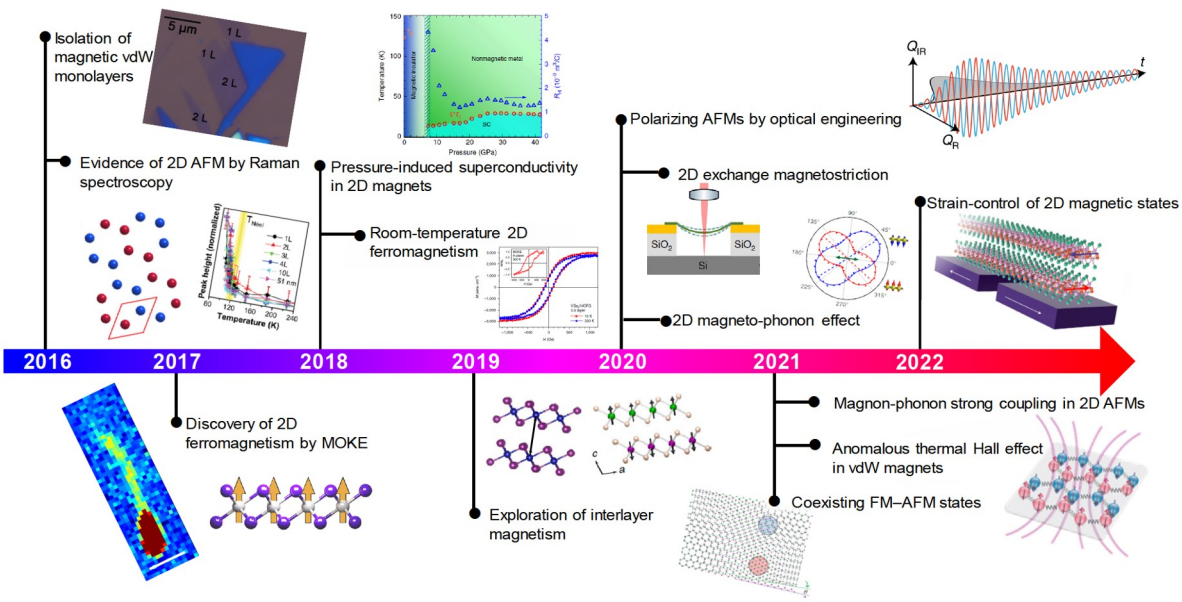

Figure 1 The timeline for spin-phonon coupling related investigations in two-dimensional magnetic materials (2DMMs). Adapted with permission from [12,18–21,26,27,30,41–47]. Copyright©2016, IOP Publishing; Copyright©2020, Springer Nature; Copyright©2021, American Physical Society; Copyright©2019, Springer Nature; Copyright©2022, Springer Nature; Copyright©2017, Springer Nature; Copyright©2017, Springer Nature; Copyright©2016, American Chemical Society; Copyright©2015, American Chemical Society. Copyright©2018, The Author(s). Copyright©2018, Springer Nature; Copyright©2019, Springer Nature; Copyright©2020, Springer Nature; Copyright©2020, Springer Nature; Copyright©2021, American Association for the Advancement of Science.

coupling effects; at last, we will briefly discuss device developments and concepts based on spin-phonon coupling.

The development of spin-phonon coupling investigation in 2DMMs

Synthesis and assembly

The 2D materials with atomic-scale thickness can be obtained by two strategies: one is bottom-up including chemical vapor deposition (CVD) and molecular beam epitaxy (MBE); the other is top-down approach know as mechanical exfoliation from bulk crystal. Mechanical exfoliation from bulk crystal is a facile method, which can make samples with high crystalline quality and good repeatability. Thus, we will summarize the bulk crystal synthesis of 2D magnets in Table 1. Most of the 2D magnets can be synthesized by solid-state reaction in sealed quartz tubes such as chemical vapor transport (CVT) and flux methods.

Recently, 2D hybrid organic-inorganic perovskite (HOIP) is a kind of popular materials due to its quantum-well-like structures and abundant composition combination [48]. The design of the organic cation and metal ion would endow 2D HOIP with fruitful properties including magnetism. For example, $AMCl_4$ (A = organic cation; M = Fe, Mn, Cr, and Cu), a relatively new family of 2D HOIPs, extracted considerable attention due to the presence of magnetism [49]. Furthermore, if we choose a suitable organic cation in magnetic 2D HOIPs, we can introduce ferroelectricity in the same crystal to obtain the multiferroicity in 2D limits [49–53]. Even though 2D HOIPs can be mechanically exfoliated [54], the magnetic properties of atomically thin 2D HOIPs are rarely reported. The replaceable organic cations, metal ions and (pseudo) halogen provide a broad prospect for the investigations of magnetism in 2D HOIP.

The coupling among charge-lattice-spin degrees of freedom in 2DMMs

Electric, lattice and magnetic properties of 2DMMs

2DMMs have a wide variety of electronic structures [4,107–109]. With the fast expansion of their family members in recent years, 2DMMs have so far covered insulators, semiconductors, metals and semimetals, providing fertile material resources and a rich toolbox for fabricating spintronic and magnonic functional devices. The insulating ferromagnetic chromium trihalides CrX_3 (X = I, Br, Cl) have electronic bandgaps in the range of 1.2–3.1 eV [110]. Similarly, the optical bandgaps of insulating antiferromagnetic MPX_3 (M = Mn, Fe, Ni; X = S, Se) range from 1.3 to 3.5 eV [41]. In contrast, the ferromagnetic $Cr_2X_2Te_6$ (X = Ge, Si) are semiconducting with smaller bandgaps of ~0.4 eV, and ferromagnetic Fe_3GeTe_2 is metallic [111]. Due to the reduced electromagnetic screening of 2D materials, 2DMMs also show various intriguing electronic properties, such as increased electron correlation, large exciton binding energy, and flexible control of charge concentrations by electrostatic gating [28].

Due to the 2D lattice structures, the electronic and magnetic properties of 2DMMs are determined by both intralayer strong covalent bonds and interlayer weak van der Waals interactions, the latter of which has been paid more attention since the interlayer coupling is an important tuning knob to modulate the fascinating properties in 2DMMs. Most of the 2DMMs are readily to be exfoliated into monolayer of atomic thickness. The large interface-to-volume ratio of thin 2DMMs makes it plausible to modify the properties of 2DMMs

Table 1 Single-crystal synthesis for van der Waals magnetic materials (The type of magnets is divided based on the experimental or theoretical results. The priority concerning the classification is given to the experimental methodologies.)

Type of magnets	Crystal	Transport agent/reaction	Temperature (°C)	Ref.
Ferromagnets	$Cr_2Ge_2Te_6$	Te self-flux	700	[55]
	$Cr_2Si_2Te_6$	Te self-flux	500	[56]
	Fe_3GeTe_2	I_2	750–700	[57]
	VTe_2	I_2	900–810	[58]
	VSe_2	I_2	820–720	[58]
	VS_2	I_2	900–850	[59]
	$MnSe_2$	ICl_3	600–540	[59]
	CrI_3	Auto transport	630–550 650–350	[60] [61]
	$CrBr_3$	Auto transport	750–200 →750–650	[33]
	GdI_2	Auto transport	827	[62]
	VI_3	Auto transport	650–550	[63]
	VS_2	I_2	900–850	[64]
	InP_3	Auto transport	1200	[65]
	GaSe	Auto transport	990–850	[66]
	GaS	I_2	850–750	[67]
	α-MnO_2	KOH	650	[68]
Antiferromagnets	$FePS_3$	I_2	650–600	[41]
	$FePSe_3$	I_2	650–600	[41]
	$MnPS_3$	I_2	650–600	[41]
	$MnPSe_3$	I_2	650–600	[41]
	$NiPS_3$	I_2	650–600	[41]
	$NiPSe_3$	KCl-$AlCl_3$ flux	–	[69]
	$CuCrP_2Se_6$	$SeCl_4$	650–600	[70]
	$AgCrP_2S_6$	I_2	800–750	[71]
	$AgVP_2S_6$	Auto transport	600	[72]
	$CrSe_2$	Oxidation of K_xCrSe_2(X~1) with iodine in acetonitrile		[73]
	$CrTe_2$	Oxidation of $KCrTe_2$ with iodine in acetonitrile		[74]
	$CrTe_3$	KCl-$AlCl_3$ flux	450–425	[75]
	$Ni_3Cr_2P_2S_9$	Auto transport	800	[76]
	$MnBi_2Te_4$	I_2	590	[77]
	$MnBi_2Se_4$	I_2	800–700	[78]
	$CrCl_3$	Auto transport	720–600	[79]
	$FeCl_2$	$AlCl_3$	350–250	[64]
	$FeBr_2$	Ar	500	[80]
	FeI_2	I_2	550	[81]
	$MnBr_2$	Br_2+Mn in ether	Room temperature	
	$CoCl_2$	$AlCl_3$	400–300	[64]
	$CoBr_2$	$AlBr_3$	345–245	[64]
	$NiCl_2$	$AlCl_3$	350–300	[64]
	VCl_2	I_2	350–400	[82]
	VBr_2	I_2	350–400	[82]
	VI_2	I_2	580–520	[64]
	$FeCl_3$	Cl_2	593→575–588	[83]
	$FeBr_3$	Br_2	150–200	[84]
	CrOCl	Cl_2	940–840	[64]
	FeOCl	I_2	400–380	[85]
	VOCl	Auto transport	1030–980	[86]
	CrSBr	Br_2	700–900→900–850	[87]
	$MnCl_2$	$AlCl_3$	400–350	[64]
	VCl_3	Cl_2	300–250	[64]
	VBr_3	Auto transport	480	[88]
	$AFeCl_4$ (A = organic cation)	Self-assemble in solution	Room temperature	[89,90]
	$AMnCl_4$ (A = organic cation)	Self-assemble in solution	Room temperature	[91]

(*To be continued on the next page*)

(*Continued*)

Type of magnets	Crystal	Transport agent/reaction	Temperature (°C)	Ref.
Multiferroics	$CuCrP_2S_6$	Auto transport	650–600	[70]
	$CuCl_2$	$AlCl_3$	450–350	[64]
	$CuBr_2$	CuO + HBr solution	Room temperature	[92]
	$NiBr_2$	$AlBr_3$	345–245	[64]
	NiI_2	I_2	750–700	[93]
	CoI_2	I_2	500–425	[93]
	MnI_2	I_2	590–420	[94]
	SnO	$SnCl_2 \cdot 2H_2O$ + NaOH hydrothermal	180	[95]
	GeS	I_2	863–788	[96]
	GeSe	I_2	570–450	[97]
	SnS	I_2	950–850	[98]
	SnSe	Auto transport	790–740	[99]
	GaTeCl	Auto transport	260–270	[100]
	CrN	Cr-Ga-Na	850	[101]
	CrB_2	Al	1550	[102]
	$ACuCl_4$ (A = organic cation)	Self-assemble in solution	Room temperature	[49–51]
	$ACrCl_4$ (A = organic cation)	Self-assemble in solution	Room temperature	[52,53]
Proximate Kitaev quantum spinliquid	α-$RuCl_3$	Cl_2	550	[103]
Half metals	MnF_3	F_2	500	[104]
	MnSSe	I_2	945–850	[64]
	$TiCl_3$	$AlCl_3$	300–250	[64]
Spin-Peierls	TiOCl	HCl,$TiCl_3$	650–800→520–600	[105]
	TiOBr	Br_2	650–550	[106]

through proximity or interface effect. 2DMMs also exemplify good mechanical flexibilities, with magnetic properties hinged on structural parameters, suggesting a possibility to apply tensile and compressive strain to modulate new functionalities [28]. Since there are no dangling bonds on the surface, it is convenient to stack 2DMMs with the same or different compounds to form homo- or heterostructures with desired special properties and functions. 2DMMs can also form superlattice structures to investigate the strong coupling between light and matter [112]. The rotational angle between adjacent layers becomes a meaningful knob to tune the interlayer couplings. With moiré patterns formed, magnetic domains with different magnetic orders can be obtained in a single heterostructure [113].

The magnetism of 2DMMs comes from the directional arrangement of spin angular momentums of unpaired electrons in magnetic ions. According to spin dimensionality n, 2DMMs can be grouped into Ising, XY and Heisenberg types with n = 1, 2, and 3, respectively. Till now, there are several magnetic phases observed experimentally in 2D materials, such as ferromagnetic phases, antiferromagnetic phases, spin liquids, magnetic skyrmions, and so forth. According to the in-plane magnetic order, 2DMMs can be divided into intralayer ferromagnets and antiferromagnets. Determined by the 2D lattice structure, the magnetic screening effect in 2DMMs is generally weak compared to 3D magnets. Thus the magnetic properties of 2DMMs can be readily tuned by the external magnetic field or proximity effect making it possible to fabricate 2DMM-based spintronic or magnonic devices with low-energy cost [4].

Charge-lattice-spin coupling in 2DMMs

The 2D lattice structure is the main physical origin of the quantum confinement of 2DMMs, leading to layer-

dependent and direction-dependent thermal, optical, electronic and magnetic properties. Therefore, the behavior of the lattice dimension in 2DMMs is naturally coupled with its electron and spin degrees of freedom. Since most of the 2DMMs contain magnetic ions with partially-filled d-orbitals, the arrangement of electrons and spins in d-orbitals determines the magnetism, which has been experimentally verified [114,115]. According to the Mermin-Wagner theorem, long-range magnetic order in spin-rotational invariant 2D systems does not exist [25]. However, with the existence of magnetic anisotropy, the spin-rotational invariance is broken thus the existence of long-range magnetic order becomes allowed. In 2016 and 2017, the existence of intrinsic 2DMMs is verified experimentally [12,26,27,30]. As an important component of magnetic anisotropy, single-ion anisotropy originates from the interplay of spin-orbit coupling and the crystal field. The existence of critical spin-orbit coupling couples the electron and spin degrees of freedom together, making the strong spin-charge coupling a prevailing correlation effect in 2DMMs. Therefore, the rational manipulation between the electronic properties and magnetic properties of 2DMMs can be carried out, and functional devices can be developed based on these spin-charge couplings. For example, the magnetic order of materials can be controlled by modulating the charge doping with an electrostatic gating [111]. In the spin-filter van der Waals heterostructures, the tunneling magnetoresistance is giant, which can push the magnetic information storage to the atomic thickness [116].

Spin-phonon coupling in 2DMMs

(1) Chromium trihalides (CrX_3)

CrX_3 (X = Cl, Br, and I) are among the most extensively studied 2DMMs. The oxidation state of Cr in this compound is expected to be +3, with an electronic configuration of $3s^0 3d^3$. The crystal lattice of CrX_3 is shown in Figure 2A [117]. In a single layer of CrX_3, the magnetic Cr ions form a honeycomb lattice and are sandwiched between two X layers. Bulk chromium trihalides have a rhombohedral structure with the $R3$ symmetry at low temperatures, and a monoclinic structure with the $C2/m$ symmetry at high temperatures. CrX_3 has intralayer ferromagnetic order with spin dimensionality being n = 1, 2 and 3 for X = I, Br and Cl, respectively. Bulk CrI_3, $CrBr_3$ and $CrCl_3$ have T_C at about 27, 47, and 70 K respectively [118,119], and the theoretical bandgaps of monolayer CrI_3, $CrBr_3$ and $CrCl_3$ are about 2.6, 1.33, and 1.06 eV accordingly [120]. In CrX_3 family, $CrBr_3$ and $CrCl_3$ are considered to be ferromagnetic insulators while CrI_3 is considered to be a ferromagnetic semiconductor. One of the unique features of few-layer CrX_3 is that their net magnetic moment depends on the parity of the layer numbers [10,26]. This behavior originates from their A-type anti-ferromagnetism, where the spins arrange ferromagnetically in each single layer while couple anti-ferromagnetically between neighboring layers. As a result, the magnetic moments of neighboring layers mutually offset, leading to a zero net magnetic moment in the whole CrX_3 with even layer numbers [26]. It has been found that the interlayer magnetism of CrI_3 and $CrBr_3$ depends on the layer stacking order, which can be tuned by high pressure [20]. The materials are ferromagnetic with monoclinic stacking order, while they become antiferromagnetic with rhombohedral stacking order [10]. The control of magnetism by fabricating twisted heterobilayers further demonstrates the close correlation between lattice and magnetism in CrX_3 [47]. The Raman scattering selection rule of phonons in CrX_3 is decided by the magnetic order [18], and the intensity and frequency of phonon peaks are influenced by intrinsic magnetic order and external magnetic field [33,121]. Theoretical calculations showed that the magnon-polaron could be formed by the coupling of

a topological magnon and a chiral phonon in 2D magnetic hexagonal lattice materials, thus regulating the transport properties of the magnons and the mechanical properties of the material [33,122,123].

(2) Metal phosphorus trichalcogenides (MPX_3)

The bulk MPX_3 (M = Mn, Ni, Fe; X = S, Se) has a monoclinic crystal structure. The M atoms are coordinated with six S atoms, while three S atoms and one P atom are coordinated to form a $[P_2S_6]^{4-}$ skeleton. The magnetic M ions are arranged in a 2D honeycomb structure. The crystal lattice of MPX_3 is shown in Figure 2B [41]. MPX_3 are intralayer antiferromagnets. Among them $MnPS_3$ has intralayer Néel-AFM of Heisenberg type, $NiPS_3$ has zigzag-AFM of XY-type and $FePS_3$ has zigzag-AFM of Ising type. The Néel temperatures (T_N) of $MnPS_3$, $NiPS_3$, $FePS_3$ are 78, 150, and 120 K, respectively [124]. MPX_3 have different interlayer exchange interactions with varying X. $MnPS_3$ and $NiPS_3$ have interlayer ferromagnetism while $FePS_3$ has interlayer antiferromagnetism [124]. Strong spin-phonon coupling effects have been observed in MPX_3. In $FePS_3$, the activation of zone-boundary phonons is observed due to the presence of the magnetic order [12,30]. At a strong magnetic field, the strong couplings between magnon and phonon are discovered in $FePS_3$ [19]. Similarly, the phonon frequencies show sudden shifts caused by the formation of magnetic order in $MnPS_3$ [13]. In $MnPSe_3$, the hybridization of magnon and phonons were reported [125]. Moreover, strain is found to be effective to tune the magnetic order and spin angular moment in $MnPSe_3$, indicating the existence of strong spin-phonon coupling effect [40]. In $NiPS_3$, the splitting of phonon peaks caused by magnetic order was observed [126]. Benefiting from this effect, it is found that the XXZ-type antiferromagnetism is suppressed drastically with the reduction of thickness, due to the thermal and spin fluctuations of the 2D lattice [126]. It is worth noting that $NiPS_3$ is a strongly correlated electron system, where coherent many-body excitons with a strong coupling to optical phonons have been observed in the antiferromagnetic state [127–129].

(3) Ternary compounds MXY

Bulk MXY (M = transition metal; X = O, S, Se, Te, N; Y = Cl, Br, I) has an orthogonal lattice structure as shown in Figure 2C [130]. In a single MXY layer, M_2X_2 layer is sandwiched by two Y layers, and M ions are at the center of the octahedron formed by X and Y atoms. The magnetic ions form a rectangular lattice instead of a honeycomb lattice in a single MXY layer, which is different from the case of compounds in CrX_3 and MPX_3 families. Among MXY, CrSBr [131] and CrOCl [132] were investigated extensively. CrSBr are also A-type antiferromagnets, so its monolayer counterpart is predicted to have intrinsic ferromagnetism [131]. Bulk and monolayer CrSBr has similar magnetic phase transition temperature at ~140 K, which can be probed by the variation of Raman spectra induced by the formation of magnetic structures [133]. Moreover, a strain modulation has been demonstrated to induce reversible magnetic phase transition in CrSBr [21], suggesting a strong coupling between the lattice and spin structures. CrOCl has an intralayer stripy-antiferromagnetism with $T_N \approx 14$ K and spin-density-wave (SDW) transition temperature at about 27 K [36]. X-ray diffraction shows that the magnetic phase transition is accompanied by a structural phase transition [134], indicating the existence of strong coupling between spin and lattice degrees of freedom. The strong spin-phonon coupling in CrOCl is further verified by the observation of the abrupt shift of the phonon frequencies by Raman spectroscopy at T_N [36]. Besides, in VOCl, several Raman-active modes show remarkable frequency deviations below T_N [135], which is due to strong spin-phonon coupling inside.

(4) Fe_3GeTe_2 and $Cr_2Ge_2Te_6$

Fe_3GeTe_2 (FGT) interests the research field due to its itinerant ferromagnetism with T_C higher than 200 K.

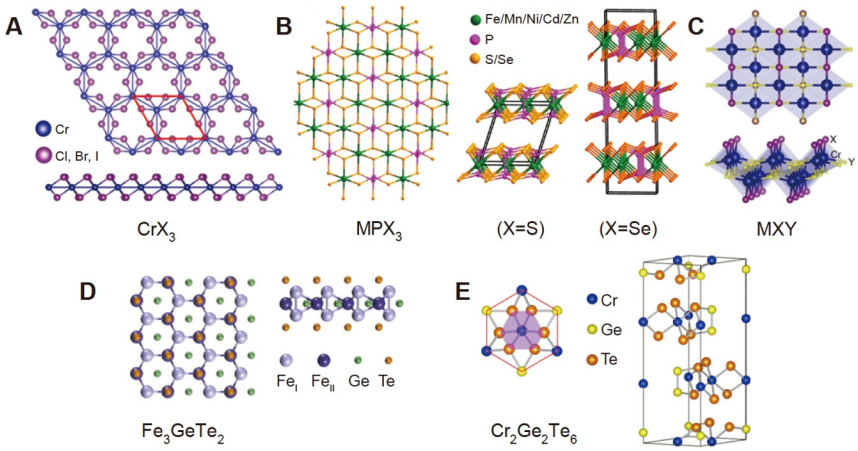

Figure 2 The lattice structure of (A) chromium trihalides CrX_3 (X = Cl, Br and I). Adapted with permission from [117]. Copyright©2018, American Physical Society. (B) Metal phosphorus trichalcogenides MPX_3 (M = Mn, Ni, Fe; X = S, Se). Adapted with permission from [41]. Copyright©2015, American Chemical Society. (C) MXY (M = transition metal; X = O, S, Se, Te, N; *Y* = Cl, Br, I). Adapted with permission from [130]. Copyright©2021, Royal Society of Chemistry. (D) Fe_3GeTe_2 and (E) $Cr_2Ge_2Te_6$. Adapted with permission from [111] and [27], respectively. Copyright©2018, Springer Nature; Copyright©2017, Springer Nature.

FGT crystallizes in a hexagonal lattice structure as shown in Figure 2D [111]. The ferromagnetism in FGT has been verified to maintain from bulk down to monolayer [136]. Notably, the T_C of FGT can be tuned to room temperature by electrostatic gating, implying its great application potential in spintronics [111]. Moreover, the spin-phonon coupling in FGT modifies the phonon energy and gives rise to enhancement of Raman susceptibility under magnetic order [31]. It is also found that the ferromagnetism in FGT can be tuned by applying strain [14]. By selecting different substrates, the T_C of layered FGT can be modulated significantly due to the lattice distortion and charge redistribution between the interfaces [137].

$Cr_2Ge_2Te_6$ (CGT) is a ferromagnetic insulator. The magnetic ions Cr in a single layer form a honeycomb lattice. The crystal lattice of CGT is shown in Figure 2E [27]. Bulk CGT possesses both interlayer and intralayer ferromagnetic coupling. When the thickness increases from bilayer to bulk, T_C increases from 30 to 70 K. Raman study uncovers strong spin-phonon coupling in CGT [29] by observing phonon modes splitting and phonon energy upturn with the formation of ferromagnetic order. In monolayer CGT, theoretical calculations show that certain specific phonon modes couple with spins intensively and modulate the direct exchange interaction between Cr-Cr [17]. Recently, Zhu *et al*. [138] found experimentally that the significant anisotropic lattice constructed by the interlayer van der Waals force and the intralayer covalent bond can induce anisotropic spin-orbit field and the spin orientation-dependent band splitting in CGT, indicating that spin-phonon coupling has a profound influence on the magnetic and electric properties of CGT.

Theoretical investigations of spin-phonon coupling in 2DMMs

The lattice parameters involving the magnetic ions could influence the magnetic order drastically. The spin-phonon coupling has been investigated theoretically in 2DMMs which provides important guidelines and explanations for experimental investigations. Typically, the total energies of different magnetic phases can be calculated and compared to predict the most stable magnetic order with specific lattice structures or atomic

displacements [139]. The first-principle density functional theory (DFT) calculations have been conducted to investigate the spin-phonon coupling effect in 2DMMs. For example, on the basis of the electronic and magnetic structure calculated by DFT method, the tensile and compressive lattice changes (estimated from the applied strain) were given to $MnPSe_3$ [140]. In detail, the energy difference between the ferromagnetic and the antiferromagnetic states is calculated to estimate the stability of the antiferromagnetic order, and a large strain of ~13% is predicted to induce a phase transition from the antiferromagnetic to the ferromagnetic states [140] as is shown in Figure 3A. The interesting stacking-order-dependent magnetism in bilayer CrI_3 was also well explored by calculation. The modulation of interlayer exchange interactions by lattice stacking is uncovered, which uncovered that the AB-stacking stabilizes a ferromagnetic state, while AB'-stacking stabilizes an antiferromagnetic state [10] (Figure 3B). Webster *et al*. [11] calculated the phonon dispersion and partial phonon density of states of CrI_3 monolayer in the antiferromagnetic and the ferromagnetic orders, indicating a clear influence on the phonon properties from the magnetic orders (Figure 3C). They also observed a visible shift of the optical phonon branches between the two magnetic states, suggesting a strong spin-phonon coupling in CrI_3. Besides that, the calculation study of $Cr_2Ge_2Te_6$ suggests that the ferromagnetic state becomes more stable when the lattice is stretched [17]. Go *et al*. [16] theoretically investigated the magnon-phonon hybridization in 2D ferromagnets, and concluded that the magnon-polarons are topologically nontrivial and their topological properties can be tuned by the external magnetic field. For monolayer Fe_3GeTe_2, Hu *et al*. [14] investigated the strain-dependent total energy at different magnetic orders on optimized lattice structure with spin-polarized DFT calculation. It was revealed that the distance of Fe ions

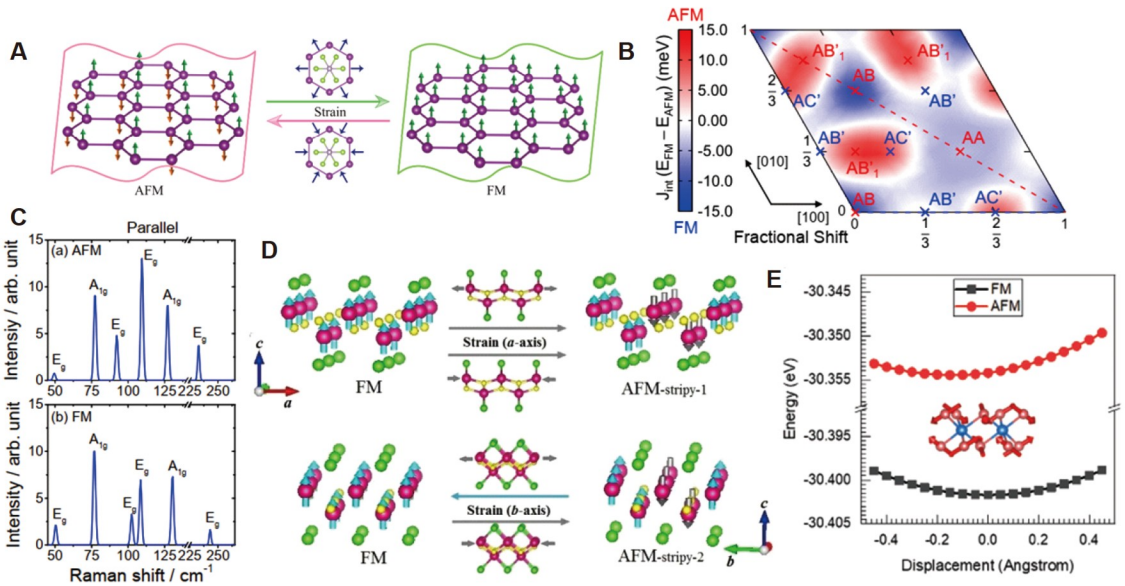

Figure 3 Theoretical investigations of spin-phonon coupling in 2DMMs. (A) Schematic of magnetic coupling change in monolayer $MnPSe_3$ induced by biaxial strain. Adapted with permission from [140]. Copyright©2018, Springer Nature. (B) The interlayer exchange energy landscape for different stacking orders in bilayer CrI_3. Adapted with permission from [10]. Copyright©2018, American Chemical Society. (C) Raman spectra of CrI_3 monolayer with parallel polarization laser setup showing different features in AFM and FM states. Adapted with permission from [11]. Copyright©2018, Royal Society of Chemistry. (D) Magnetic phase transition in monolayer CrOCl induced by uniaxial strain. Adapted with permission from [15]. Copyright©2020, Royal Society of Chemistry. (E) Calculated total energy of the ferromagnetic (black squares) and antiferromagnetic (red circles) states for the atomic displacement of certain phonon modes in the ferromagnetic monolayer $CrBr_3$. Adapted with permission from [141]. Copyright©2022, John Wiley & Sons, Inc.

and Fe–Te–Fe angles changes with the applied strain, resulting in the stability of ferromagnetic order with tensile strain. Qing *et al*. [15] used the first-principle DFT calculation to obtain the ground state of intralayer ferromagnetic order and interlayer antiferromagnetic order in unstrained CrOCl, and then theoretically predicted that the magnetic phase transition between ferromagnetic and antiferromagnetic states can be achieved by applying strains along *a*-axis and *b*-axis as is shown in Figure 3D. Other than fixing specific lattice geometry, the energy changes of magnetic phases are also calculated with respect to lattice displacement of specific phonon modes in the spin-phonon investigation of monolayer $CrBr_3$ by Wu *et al*. [141] as shown in Figure 3E. Pandey *et al*. [142] calculated the phonon dispersion between different magnetic states in monolayer $CrBr_3$ and CrI_3, and investigated the strain-dependent thermal conductivity to figure out the relation between the strong spin-phonon coupling and phonon transport in two types of materials. Similarly, Liu *et al*. [143] theoretically investigated how the spin-phonon coupling affects the geometric structure, phonon frequency, thermal transport, and magnetic stability of magnetic semiconductor monolayers of MX_3 (M = Fe, Ru; X = Cl, Br, I) and CrI_3, which uncovers the important role the spin-phonon coupling played on thermal transport properties. The theoretical investigations of spin-phonon coupling in 2DMMs provide rich information and insights on uncovering magnetism-mediated thermal and mechanical properties, which is beneficial to magnetism engineering by modifying the lattice or phonon excitations.

Variation of phonon properties with magnetic order in 2DMMs

Phonons are quanta of lattice vibration. Raman spectroscopy is a powerful experimental method to detect the phonon properties and their interplay with other quasiparticles in condensed matter [144]. Due to energy and momentum conservation, Raman spectroscopy usually probes the inelastic scattering between electrons and zone-center optical phonons, since the momentum of photons is much smaller compared with the lattice momentum. The phonon modes are generally sensitive to the structural phase transition, as well as other variations of lattice structure (i.e., symmetry or dimensionality changes or defects/disorders in lattices), manifested as variations of important spectroscopy parameters such as peak position, intensity and linewidth. In contrast, phonons are usually insensitive to the magnetic ordering in most of materials. However, benefiting from the various spin-phonon coupling, phonon can become a meaningful probe to examine the spin properties by optical spectroscopy methods.

Emerging phonon modes with magnetic ordering

Since the achievement of atomically thin layers of van der Waals magnetic crystals in early 2016, the effort has been devoted to searching the long-range magnetic ordering in “true” 2D systems [41]. In order to obtain clear evidence of the persistence of magnetic properties down to monolayer thickness, early investigations are focused on seeking significant signatures accompanied by the magnetic phase transition by electrical or optical measurements. The breakthrough was from the Raman spectroscopy studies of monolayer $FePS_3$ by Wang *et al*. [12] and Lee *et al*. [30]. Without any structural phase transition happening, the specific zigzag antiferromagnetic ordering of $FePS_3$ results in a primitive cell expansion and a concomitant Brillouin-zoom folding when the materials transit from the paramagnetic phase to the antiferromagnetic phase. As a result,

when the temperature goes across its T_N (~118 K), an asymmetric and broad peak at ~100 cm^{-1} can be observed in the paramagnetic phase, while it splits into two symmetric peaks at ~88 and 95 cm^{-1} at antiferromagnetic phase (Figures 4A and 4B). By tracking the characteristic Raman mode, a magnetic phase transition can be experimentally verified in monolayer $FePS_3$ [12,30]. The case is not limited to antiferromagnets. Tian *et al*. [29] observed strong spin-phonon coupling effects prevailing down to few-layer ferromagnet—$Cr_2Ge_2Te_6$, where a peak splitting arises as the temperature goes down across T_C (Figure 4C). The splitting of the E_g peak is ascribed to the time-reversal symmetry breaking by the spin ordering.

Spin-phonon coupling provides an effective way to detect the magnetism in 2D layers and launches the early exploration on 2D magnetism via Raman spectroscopy before the discovery of 2D ferromagnetism in monolayer CrI_3 and bilayer $Cr_2Ge_2Te_6$ by MOKE [26,27], which has sparked tremendous interest in magnetism in 2D monolayer limit. After that, spin-phonon coupling continues to play a significant role in the

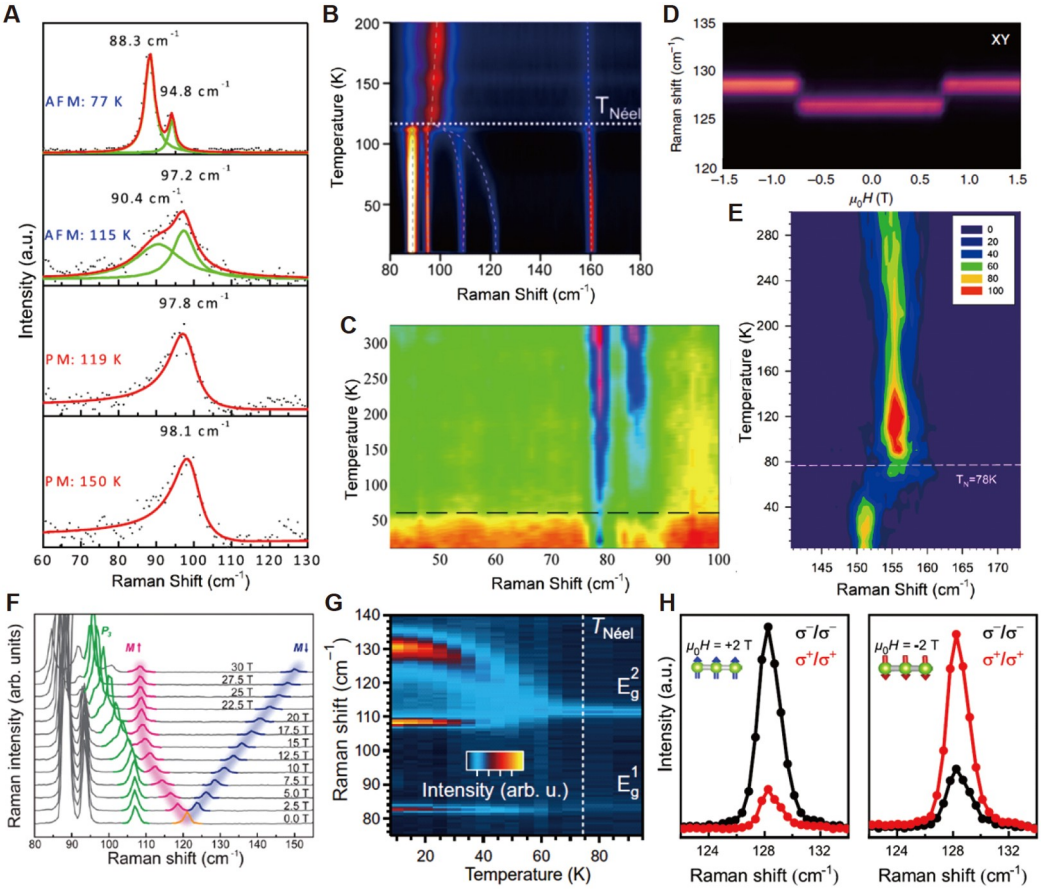

Figure 4 Variation of phonon properties with magnetic order in 2DMMs. (A) Evolution of zone-boundary phonon in monolayer $FePS_3$ by Raman spectroscopy. Adapted with permission from [12]. Copyright©2016, IOP Publishing. (B) Temperature-dependent Raman spectra in monolayer $FePS_3$ around T_N. Adapted with permission from [30]. Copyright©2016, American Chemical Society. (C) Temperature-dependent Raman spectra in few-layer $Cr_2Ge_2Te_6$ near T_C. Adapted with permission from [29]. Copyright©2016, IOP Publishing. (D) Magnetic-field-dependent Raman mode of bilayer CrI_3 in the cross-linear scattering channel. Adapted with permission from [18]. Copyright©2020, Springer Nature. (E) Variation of phonon energy at around T_N in $MnPS_3$. Adapted with permission from [13]. Copyright©2019, American Chemical Society. (F) Magnon-phonon strong coupling in $FePS_3$ at high magnetic fields. Adapted with permission from [19]. Copyright©2021, American Physical Society. (G) Hybridization of two-magnon excitations with two phonons in $MnPSe_3$. Adapted with permission from [125]. Copyright©2021, The Author(s). (H) Probing the ferromagnetism and spin wave gap in VI_3 by helicity-resolved Raman spectroscopy. Adapted with permission from [32]. Copyright©2020, American Chemical Society.

investigation of spin properties and their coupling to various excitations in 2DMMs. Similarly, as a semiconductor isostructural to the MPS_3 system, $Cr_2Ge_2Te_6$ is a Heisenberg ferromagnet with weak out-of-plane anisotropy below its T_C of 68 K. Raman measurements on exfoliated thin flakes also suggest the presence of spin-phonon coupling and the suppression of magnetic quasi-elastic scattering [107].

Apart from the temperature-induced magnetic phase transition, the application of external magnetic fields is another common, even more direct way to change the spin orders in the materials. Therefore, the investigations of magnetic-field-dependent phonon behaviors are also important approaches to studying the spin-phonon coupling. Padmanabhan *et al*. [145] reported the interlayer magnetophotonic coupling in the layered magnetic topological insulator $MnBi_2Te_4$. The anomalies in phonon scattering intensities were observed across a magnetic-field-driven phase transition, which is a spin-flop transition from a layered antiferromagnetic ground state to a canted antiferromagnetic state with an out-of-plane magnetic field of about 3.5 T [107]. When the spins in $FePS_3$ order below T_N, several phenomena can be observed with an application of out-of-plane external field, including the appearance of a new Raman mode at around 110 cm^{-1} at magnetic field $B > 2$ T and a clear splitting of 122 cm^{-1} peak from 0 to 9 T [146].

Besides the detection of spin-phonon coupling in 2D limits, Raman spectroscopy also offers the possibility to probe a variety of excitations in 2D magnets. Jin *et al*. [60] reported spin wave excitations in the 2D Ising honeycomb ferromagnet CrI_3 by polarized micro-Raman spectroscopy studies. The definitive evidence of two sets of zero-momentum spin waves at frequencies of 2.28 and 3.75 terahertz (THz) is demonstrated. Different from bulk antiferromagnets, 2D CrI_3 couples efficiently with external magnetic fields, where two branches of THz spin waves with their lifetime on the order of 10–100 ps are identified.

The variation of phonon polarization induced by spins

As an important feature of phonon, the Raman polarizability also exhibits substantial variations when the magnetic phase transition occurs in some specific 2D magnets with giant magneto-optical effects. In a fix polarization configuration, the relative Raman peak intensity of the A_g^2 mode of $CrBr_3$ significantly changes with the increase of the magnetic field, in contrast to the field-independent behavior of E_g mode [33]. Several research groups [18,147–149] have discovered the giant magneto-optical effect of Raman mode, i.e., A_g^1 mode located at ~130 cm^{-1}, in atomically thin CrI_3. Such magneto-phonon coupling results in a rotation of the polarization angle of Raman signal, which reaches around two orders of magnitude larger than that of MOKE signal [18,147]. Specifically, a sudden change of peak intensity in the cross-polarization configuration can be observed when a field-driven spin-flip occurs in monolayer CrI_3, while a clear peak shift of ~2 cm^{-1} was captured when the spin orders are switched between the ferromagnetic and the antiferromagnetic sequences in bilayer CrI_3 (Figure 4D). In addition, Raman spectroscopy can also be applied in the detection of magnetic sequence transitions in CrI_3 with larger layer-number, although this polarization anomaly becomes weaker as the number of layers increases. Similar effects can be found in 2D ferromagnetic VI_3 [32].

Kim *et al*. [126] utilized Raman spectroscopy to report a suppression of magnetic ordering in antiferromagnetic monolayer $NiPS_3$, which is in stark contrast to the case in $FePS_3$ [12,30]. This result is based on the splitting of low-frequency modes at ~180 cm^{-1} and its variation of Raman polarizability due to the presence of XXZ-type magnetic ordering, which is absent in the monolayer samples. As mentioned above, Sun *et al*. [146] observed a new phonon mode at ~110 cm^{-1} at $B > 2$ T, whose polarization depends on the

magnetic field. This phenomenon suggests a special polarization coupling mechanism arising from spin-phonon coupling, which contributes a significant modification to the Raman tensor under the magnetic field.

Phonon frequency variation induced by spins

The study of Sun *et al*. [13] demonstrated a clear shift of Raman peak with the onset of antiferromagnetic orders in $MnPS_3$ when the temperature goes across its T_N (Figure 4E). Similarly, the Fe_3GeTe_2 phonons soften rapidly below 140 K, and the anharmonic model shows the deviation of the frequency of specific Raman-active modes due to the spin-phonon coupling caused by the modulation of the super-exchange integral by lattice vibrations [31]. A conventional hardening of phonons of $CrBr_3$ with decreasing temperature is observed due to the suppression of the anharmonic phonon-phonon interactions [33]. As a consequence, the temperature dependence of Raman features becomes much stronger with the onset of magnetic ordering below ~50 K. Choe *et al*. [38] investigated the electron-phonon scattering and spin-phonon coupling in few-layer $MnBi_2Te_4$, which results in a slight red shift of A_{1g} mode frequency when a phase transition from the paramagnetic phase to the antiferromagnetic phase occurs. In contrast to the variations of Raman peak position at the magnetic phase transition temperature, the spin-phonon coupling in some 2D magnets only induces a different temperature-dependent trend on the phonon energy. The typical experimental observation of this effect is an inflection point at T_C (or T_N) in the plot of temperature-dependent Raman frequency, such as three phonon modes (E_g^4, A_g^1 and E_g^3) in $Cr_2Ge_2Te_6$ [29] and two phonon modes (E_g^1 and A_g^2) in $CrBr_3$ [33].

Another case that the spin-phonon coupling affects the phonon frequency has been widely explored in the study of magnon-phonon strong coupling (or named magnon-polarons) in antiferromagnetic $FePS_3$. Liu *et al*. [19] and Vaclavkova *et al*. [150] observed a feature of field-driven anticrossing caused by a repulsive interaction between the magnon and phonon modes when their energies are in resonance (Figure 4F). In addition, at the field above 22.5 T, considerable redshift in phonon frequency and intensity suppression imply a possible transition to the fully polarized state [19]. Furthermore, Mai *et al*. [125] demonstrated the hybridization of two-magnon excitations with two phonons in $MnPSe_3$ through temperature-dependent magneto-Raman spectroscopy (Figure 4G).

Phonon mode intensity and linewidth affected by spins

It is well known that the lineshape profile (e.g., peak position, full width at half maximum and peak intensity) of Raman-active modes changes systematically when the temperature is varied, regardless of the magnetic or non-magnetic nature of the crystals, due to the temperature-dependent bond strength and anharmonicity. Therefore, if the phonon behaviors are truly affected by the temperature-induced magnetic phase transition, such spin-phonon coupling has to be scrutinized and carefully distinguished from the temperature-dependent lattice effect. For $FePS_3$, besides the clear activation of the zone-boundary phonon mode at ~88 cm^{-1}, the Raman mode located at ~150 cm^{-1} also exhibits a clear variation on both linewidth and intensity when the temperature goes across its T_N [12,30]. Ghosh *et al*. [151] conducted a systematic Raman study on higher-frequency phonon modes in $FePS_3$ and investigated its strong spin-phonon coupling based on the analysis of the peak feature. Yin *et al*. [33] also found that the linewidths of E_g^1 and A_g^2 phonon modes decreased dramatically with the onset of magnetic order at ~T_C. This behavior extends from the first-order phonon

scatterings to higher-order phonon scattering.

On the other hand, it is rather technical to extract the variation of linewidth and peak position of Raman-active modes due to magnetic-field-induced phase transition (hence magnetic ordering), since the magnetic field hardly affects the crystalline structures. Webster *et al*. [152] demonstrated that the frequency and intensity of the Raman peak are strongly dependent on the magnetic order through the first-principles calculations of phonon properties of single-layer CrI_3, which indicates that the intensity of phonon modes is sensitive to the magnetic order. In the experiment, Lyu *et al*. [32] reported that the magnetic orders can greatly affect the Raman scattering characteristics of optical phonons in 2D VI_3, resulting in different scattering intensities when excited by left- and right-handed circularly polarized light (Figure 4H). Lyu *et al*. [32] also reported a spin-wave gap induced by the large magnetic anisotropy in this material, based on the observation of quasi-elastic scattering in the paramagnetic phase, which evolves into the acoustic magnon mode at 18.5 cm^{-1} in the ferromagnetic phase.

The phonon dynamics modulated by spins

Magnetic order in 2DMMs such as CrI_3, $MnBiTe_3$, $FePS_3$, $NiPS_3$ and $MnPSe_3$ is proved to be strongly related to many-body interactions within each layer and interlayer interactions between layers [115,153–161]. To understand the fundamental physics of these magnetic materials, steady-state optical spectroscopy measurements like photoluminescence and Raman spectroscopy are widely used. Except for these traditional methods, ultrafast spectroscopy has drawn more and more attention due to its unique capabilities in extracting the ultrafast dynamics down to sub-100 fs temporal resolution.

$FePS_3$, a 2D Ising antiferromagnet on a honeycomb lattice, is one of the most promising materials for a number of magnetic applications in spintronics and magnonics [162,163]. Using ultrafast magneto-optical spectroscopy as shown in Figure 5A, a strong divergence in the demagnetization time is observed near the T_N [156]. The rise and decay time of the time-resolved optical rotation signal both peak at T_N, at which the magnetic order is sensitive to small perturbations. The typical slowing-down of spin dynamics is due to the spin-spin interaction at the critical temperature and the longer decay time is attributed to the quasi-equilibrium systems of magnons and phonons equilibrating with the substrate. Moreover, the amplitude of the time-resolved optical rotation signal also peaks at T_N, which further confirms the magnetic phase transition process. Later, the magnon-phonon hybridization mode is excited and investigated by the ultrafast pump-probe spectroscopy [164] as shown in Figure 5B, taking a step closer in controlling magnetic order optically in $FePS_3$. $NiPS_3$, a van der Waals layered magnet with XXZ-type antiferromagnetism, is an intriguing example of a strongly correlated 2D magnet because of the energetic competition between charge transfer and Coulomb repulsion [145,165]. By selective pumping of orbital resonances with ultrashort pulses, magnetic anisotropy, which can stabilize the long-range spin order, is well controlled, resulting in the successful manipulation of its magnetic order [115], revealing strong spin-charge coupling in $NiPS_3$. Besides the direct interaction between spins and phonons, spin-phonon coupling can be also realized indirectly through suitable intermediate particles or quasi-particles in 2D materials. By photoexciting the spin-orbit-entangled excitons which originate from Zhang-Rice states in $NiPS_3$, a transient metallic state with long-range antiferromagnetism is realized [127]. The many-body excitons in $NiPS_3$ also exhibit strong coupling to optical phonons, and bridge the significant correlation between spins and phonons [159] as shown in

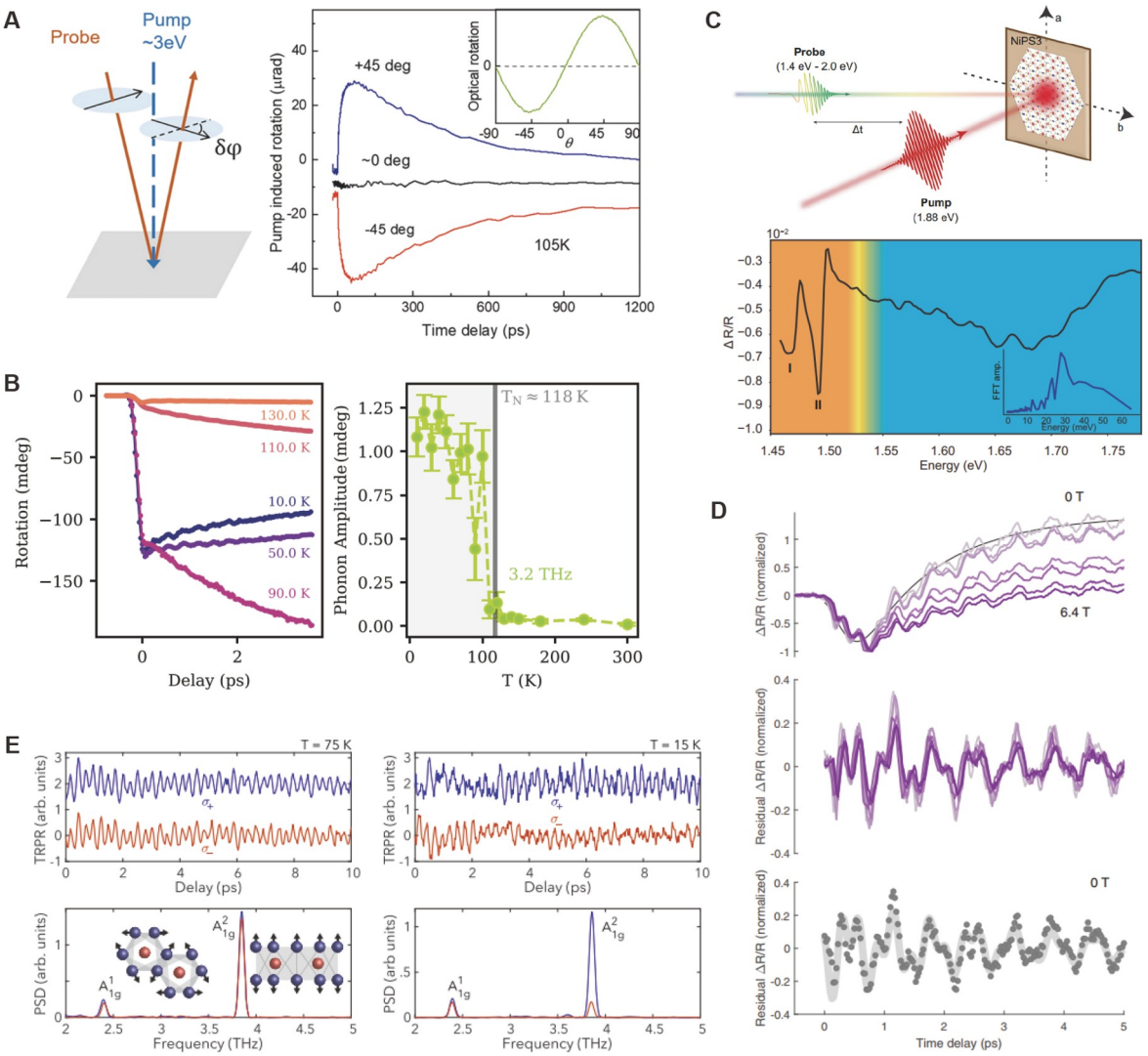

Figure 5 Revealing spin-phonon coupling by ultrafast spectroscopy in 2DMMs. (A) Time-resolved optical rotation of the probe beam detecting the spin dynamics mediated by phonon in $FePS_3$. Adapted with permission from [156]. Copyright©2021, American Chemical Society. (B) Amplitude of 3.2 THz phonon mode of $FePS_3$ by measuring transient rotation. Adapted with permission from [164]. Copyright©2022, John Wiley & Sons, Inc. (C) Phonon replica of spin-orbit-entangled exciton detected in $NiPS_3$ by ultrafast spectroscopy. Adapted with permission from [159]. Copyright©2022, The Author(s). (D) Ultrafast signatures of magnetophononic coupling in $MnBi_2Te_4$. Adapted with permission from [145]. Copyright©2022, The Author(s). (E) Coherent spin-coupled phonon dynamics in CrI_3. Adapted with permission from [161]. Copyright©2022, The Author(s).

Figure 5C. As a result, many-body exciton physics could be systematically investigated through a variety of spectroscopy approaches, including photoluminescence, Raman, and ultrafast spectroscopy [128,129,155].

Ultrafast spectroscopy has been proved as a powerful method to study the many-body interaction in 2DMMs. It can also be applied to explore the interlayer interaction among these layered materials. $MnBi_2Te_4$, a layered crystal that exhibits exotic quantum physics, is a novel magnetic topological insulator [166]. Using time-resolved pump-probe reflectivity spectroscopy, coherent phonon oscillations from the interlayer breathing mode are observed and the coherent oscillation frequency, the photocarrier and coherent phonon decay rates are found strongly related to the interlayer coupling [158]. It is reported that the interlayer

magnetic ordering can drive phase transitions between quantum anomalous Hall and axion insulator states in $MnBi_2Te_4$. Furthermore, by exploiting the strong coupling of A_{1g} phonons to exchange interaction, it is possible to control the interlayer magnetic ordering in $MnBi_2Te_4$ as shown in Figure 5D [145]. Moreover, in bulk CrI_3, strong transient exchange-mediated spin-phonon interactions are reported using ultrafast optical spectroscopy, highlighting the ultrafast magnetism control via spin-phonon coupling as shown in Figure 5E [161].

Manipulating magnetic order through spin-phonon coupling

The control of magnetism with low-energy cost and high speed is crucial for driving 2DMMs from laboratory to industrial scale. The ubiquitous spin-phonon coupling in 2DMMs provides a feasible route to achieve magnetism-tuning conveniently. With the rapid expansion of the 2DMMs family, a variety of spin-phonon coupling effects have been theoretically suggested and experimentally revealed. In this context, attempts and realizations of controlling the magnetic ordering in 2DMMs via spin-phonon (i.e., magnetic-lattice) coupling are also accumulating rapidly. The main controlling approaches include pressure, strain, and van der Waals engineering, whose representative investigations are listed in Figure 6.

Pressure tuning

As a key factor to determine magnetic order in 3D magnets, the exchange interactions between spins are strongly dependent on chemical bond lengths and angles, which can be well tuned by applying pressure. In contrast to the 3D case, the van der Waals interaction and interlayer exchange coupling in 2DMMs play a significant role in determining their magnetic properties. As a consequence, the application of pressure is expected to be an effective way to modulate the magnetism in 2DMMs, especially whose interlayer exchange interaction relies sensitively on the interlayer coupling, through the control of van der Waals gap distance and stacking order. For $FePS_3$ with typical 2D Ising antiferromagnetism at atmospheric pressure, Wang *et al*. [42] applied the high pressure on $FePS_3$ and induced 3D magnetism together with large in-plane lattice collapse, abrupt spin-crossover, and insulator-metal transition. Astonishingly, with the suppression of long-range magnetic order, $FePS_3$ shows superconducting transition at 9 GPa, implying the potential relation between 2D magnetism and superconductivity [42] as shown in Figure 6A. In some specific cases, the new structural phases and consequent magnetic phases can generate in 2DMMs at high pressure in $FePS_3$ as shown in Figure 6B [167]. The pressure-modulation of interlayer magnetic order was also achieved in extensive studies on CrI_3[20,44]. Theoretical research shows that the interlayer exchange correlation of CrI_3 strongly depends on the interlayer distance [168], which was then realized by high-pressure experiment. With the application of high pressure, magnetic circular dichroism (MCD) spectra showed that the CrI_3 bilayer transformed from antiferromagnetic to ferromagnetic states, accompanied by a structural transition from the monoclinic to the rhombohedral phases [44] as shown in Figure 6C. Notably, high pressure can effective tune the interlayer antiferromagnetic coupling strength in CrI_3 by nearly 100% [20]. In addition, the pressure-modulation of magnetism also depends on the number of layers in certain 2DMMs, such as in $MnBi_2Te_4/(Bi_2Te_3)n$ system. Under high pressure, the interlayer antiferromagnetism maintains when $n = 1$, while it

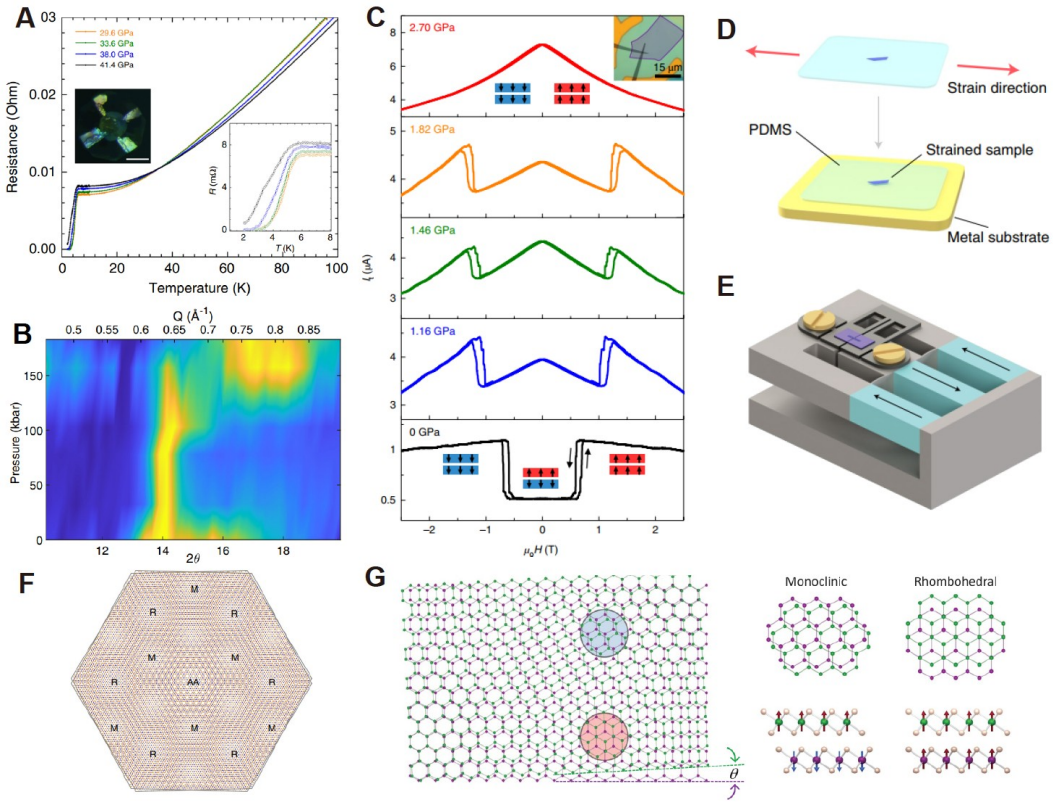

Figure 6 The magnetism tuning strategy from lattice degree of freedom. (A) and (B) Pressure tuning the magnetic phase in $FePS_3$. Adapted with permission from [42,167]. (C) Pressure tuning the stacking and magnetic phase of CrI_3. Adapted with permission from [44]. Copyright©2019, Springer Nature. (D) Strain tuning of Néel vector of $MnPSe_3$. Adapted with permission from [40]. Copyright©2021, Springer Nature. (E) Strain tuning of magnetic phase of CrSBr. Adapted with permission from [21]. Copyright©2021, Springer Nature. (F) Moiré superlattice structure of a small-twist-angle CrI_3 bilayer. Adapted with permission from [113]. Copyright©2022, Springer Nature. (G) Layer-stacking-dependent magnetic phase of CrI_3. Adapted with permission from [47]. Copyright©2021, American Association for the Advancement of Science.

changes to interlayer weak ferromagnetism when $n = 2$ [169].

To explore the multi-functional device applications of 2DMMs, it is critical to improve their T_C and coercive field strength. High pressure is not only used to induce new magnetic phase in 2DMMs in fundamental researches of condensed matter physics, but also an effective way to manipulate the original magnetic order towards enhanced magnetic phase transition temperature or coercive field strength. It is reported that $CrGeTe_3$ could transform from a ferromagnetic insulator to a ferromagnetic 2D Fermi metal under high pressure, with T_C increased intensively from 66 to 250 K [170]. The pressure-dependent behaviors become more complicated for CrI_3, whose T_C decreases with the uniaxial pressure perpendicular to the *c*-axis while increasing with the uniaxial pressure parallel to the *c*-axis [171]. Another important research direction in high-pressure magnetism is to effectively generate and systematically investigate new quasiparticles consisting of magnons and other particles, such as phonons, photons, and excitons. Such new magnon-related quasiparticles are important for magnonics and spintronics, since they might influence the transport of magnons intensely. Under high pressure, the frequencies of certain phonon modes can be specifically adjusted to resonate with that of the magnon, thereby causing the hybridization of the phonon and the magnon to form magnon polaron [172].

Strain tuning

Similar to pressure modulation, the application of strain, which is mainly the in-plane strain in 2D layers, can also change the lattice constant, thereby modulating the intralayer or interlayer exchange or super exchange interactions to achieve the modulation of magnetism in 2DMMs. Controlling magnetism by strain can be investigated by theoretical calculations. The theoretical study on $MnPSe_3$ showed that the biaxial strain can cause a magnetic phase transition from the antiferromagnetic to the ferromagnetic phases. Moreover, the strain-tuned in-plane ferromagnetic $MnPSe_3$ has semi-metallicity and spin-splitting conduction bands, which are beneficial to the propagation of spin-polarized carriers for potential spintronic applications [140]. It was theoretically predicted that the in-plane tensile strain can transform monolayer $CoBr_2$ from the ferromagnetic to the antiferromagnetic phases, while the compressive in-plane strain keeps the robust ferromagnetic order in monolayers [173]. In Fe_3GeTe_2, theoretical calculations also showed that the application of in-plane biaxial strain can enhance its ferromagnetism. The average magnetic moment of Fe ion was found to increase monotonously with the increase of the strain in the range from −5% to 5% [14]. Similarly, it was calculated that the uniaxial strain would induce a phase transition from the ferromagnetic to the antiferromagnetic phases, and greatly enhance T_C in CrOCl [15].

The regulation of magnetic order by strain has transitioned its frontier from theoretical calculations to experimental realizations recently. Ni *et al*. [40] reported a precise modulation of the Néel vector in $MnPSe_3$ by applying the uniaxial strain. When the strain reaches 2%, the Néel vector follows the direction of the strain, which brings further possibility for flexibly constructing complex magnetic orders (Figure 6D). The increase of the coercive field is beneficial to enhance the magnetic stability of 2DMMs for the potential applications of information storage, and has been reported to be achieved by applying strains. The experimental studies have found that 3.8% in-plane strain can increase the coercive field of VI_3 to 2.6 T. Based on the DFT calculations, it is suggested that the strain dramatically increases the magnetic anisotropy [174]. Strain has also been observed to drastically alter the phase transition temperature of 2DMMs. The T_C of Cr_2Te_3 increases by 50 K under the tensile strain, while decreases by 90 K under the compressive strain [175]. The recent experimental study reported that the strain leads to reversible in-plane ferromagnetic-antiferromagnetic transitions in the air-stable A-type antiferromagnetic CrSBr (Figure 6E), making a further step towards magnetism controllability in 2DMMs [21].

van der Waals engineering

One of the most fascinating properties of 2D materials is to obtain new physical properties through van der Waals engineering, including the construction of a variety of homo- and/or hetero-structures. Moreover, extensive research studies have utilized the precise control of the twist angle between layers to form moiré superlattices for expanding the tenability of constructed 2D structures by van der Waals engineering [176,177]. In the process, new phases and new physical phenomena are created. For two-dimensional magnetic materials, van der Waals engineering introduces freedom to manipulate the magnetism by tuning the exchange interactions directly, or by manipulating the electronic properties indirectly. In van der Waals engineering, the lattice deformation can be introduced, modifying bond length and angle containing magnetic ions. As a result, the exchange and super-exchange interactions can be modulated. Van der Waals engineering

can also strongly modulate the interlayer charge transfer process, thus influence the magnetic moment of ions in two dimensional materials. It was found that H-type stacking and R-type stacking bilayer $CrBr_3$ can result in the interlayer ferromagnetic and antiferromagnetic orders respectively [39]. The reason behind the phenomena is that the interlayer coupling in bilayer $CrBr_3$ is mediated through a super exchange interaction, which is controlled by the directional hybridization between the Br p-orbitals and Cr d-orbitals. Because the bond angles and the bond lengths of the Cr–Br–Br–Cr exchange path are strongly dependent on the stacking order, the interlayer magnetism is expected to depend on the specific stacking structure [39]. In four-layer CrI_3 consisting of two bilayers with a twisted angle, the properties of the homo-bilayers depend on the twist angle. In detail, the constructed homosturcture exhibits pristine four-layer CrI_3 properties at a small twist angle, bilayer CrI_3 properties at a large twist angle, and unexpected net magnetic moment at an intermediate twist angle [178]. Moreover, it shows experimentally that the magnetism of twisted bilayer CrI_3 also exhibits a strong dependence on the twist angle. When the twist angle $\theta < 3°$, the coexistence of antiferromagnetic and ferromagnetic order emerges. When the twist angle is larger than 3°, the twisted homo-structure becomes ferromagnetic. It is suggested that the formation of the coexisting ferromagnetic and antiferromagnetic phases depends on the stacking-related interlayer interaction [113] as shown in Figure 6F. The coexistence of AFM and FM domains were directly visualized by single-spin quantum magnetometry [47] (Figure 6G).

Applications of 2DMMs and spin-phonon coupling in spintronic devices

2DMMs have the advantages of nearly ideal interface and interlayer van der Waals coupling when being integrated into complex homo- or hetero-structures, which provide a promising platform for the development of high-performance spintronic and magnonic devices [107]. They can also be further characterized and modulated by external stimuli, showing great development potential and application prospects. Based on spin-phonon coupling, the external stimuli can be designed to improve the performance of spintronic and magnonic devices. Since the giant magnetoresistance (GMR) effect was discovered in 1988 [179,180], spintronic devices such as magnetic tunnel junctions (MTJs), spin valves, and spin filters have gained rapid development, where 2DMMs have also been demonstrated with promising broad applications in recent years. For the sake of briefness, here we only briefly review the basic principles and some selected investigations in the above-mentioned device applications, as well as how spin-phonon coupling is involved and operated. Certain applications of 2D magnetic materials in spintronic devices are listed in Figure 7.

GMR generates in multilayers composed of alternating ferromagnetic and non-magnetic conductive layers, where the antiparallel alignment magnetization of adjacent ferromagnetic layers gives rise to high resistance while parallel alignment gives rise to low [179–181]. This effect was extended to fabricate MTJs consisting of two ferromagnets separated by a thin non-magnetic insulator layer to obtain flexibly tunable tunnel magnetoresistance (TMR) [182,183]. With added functionalities, the MTJs could act as spin valves (two ferromagnetic layers separated by an insulating barrier) or spin filters (two nonmagnetic layers separated by an (anti)ferromagnetic barrier) in an applied magnetic field, and be utilized in information storage devices such as magnetoresistive random access memory (MRAM).

During the fabrication of MTJs with stacked 2DMMs, an antiferromagnetic ground state would be favorable which can serve as a tunnel barrier to induce spin-filtering effects [184]. The 2D magnetic insulator

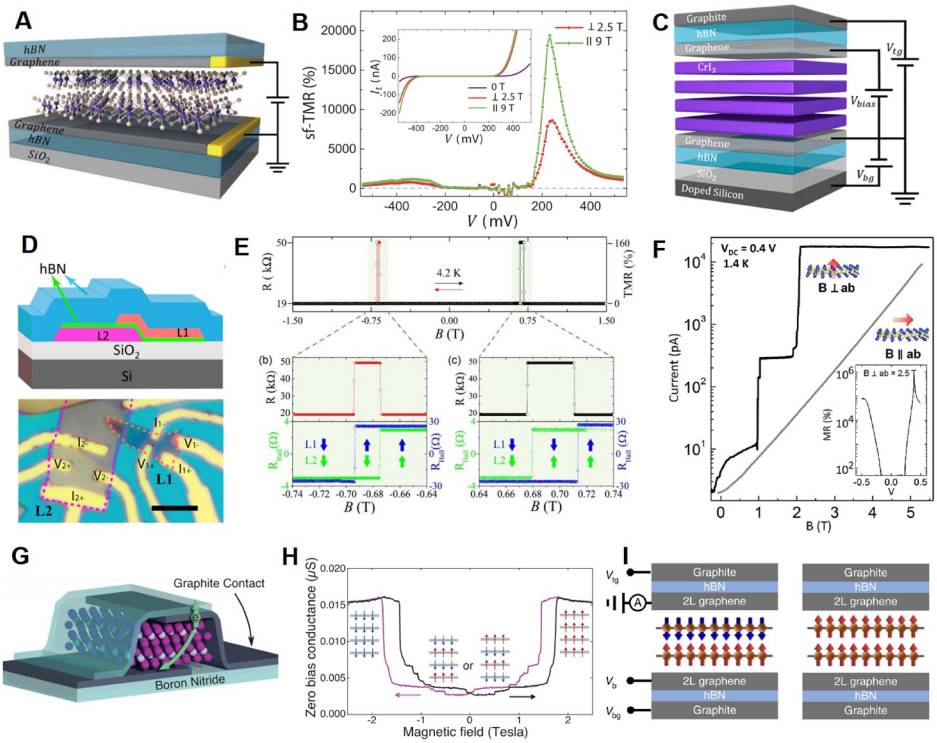

Figure 7 Applications of 2D magnetic materials in spintronic devices. (A) Schematic of 2D magnetic tunnel junction based on bilayer CrI_3 functioning as the spin-filter sandwiched between graphene. Adapted with permission from [116]. Copyright©2018, American Association for the Advancement of Science. (B) A TMR ratio up to 19,000% based on tetralayer CrI_3 MTJ. Adapted with permission from [116]. Copyright©2018, American Association for the Advancement of Science. (C) Schematic tetralayer CrI_3 MTJ with gate-tunable TMR between 17,000% and 57,000%. Adapted with permission from [189]. Copyright©2019, American Chemical Society. (D) Fe_3GeTe_2/hBN/ Fe_3GeTe_2 MTJ with hBN serving as the tunneling barrier. Adapted with permission from [6]. Copyright©2018, American Chemical Society. (E) Spin-valve effect in Fe_3GeTe_2/hBN/Fe_3GeTe_2 MTJ with TMR of 160%. Adapted with permission from [6]. Copyright©2018, American Chemical Society. (F) Current vs. magnetic field curve of CrI_3 based MTJ with TMR up to 1,000,1000%. Adapted with permission from [186]. Copyright©2018, American Chemical Society. (G) Schematic of a CrI_3-based vdW heterostructures. Adapted with permission from [185]. Copyright©2018, American Association for the Advancement of Science. (H) Conductance through a tetralayer CrI_3 tunnel barrier as a function of an out-of-plane applied magnetic field. Adapted with permission from [185]. Copyright©2018, American Association for the Advancement of Science. (I) Schematic of graphene/CrI_3/graphene MTJ with electrically controllable conductance state based on the magnetic order in the CrI_3 tunnel barrier. Adapted with permission from [190]. Copyright©2019, Springer Nature.

CrI_3 exhibits changeable ferromagnetic or antiferromagnetic orders in different layer numbers [26] and thus has been reported to be built into MTJs sandwiched between graphene electrodes [5,116,185,186] or encapsulating hBN tunnel barrier [187,188]. Song *et al*. [116] reported that a TMR of 19,000% can be reached in a CrI_3-based MTJ sandwiched between graphene at low temperature. They later investigated gate-tunable TMR of similar four-layer CrI_3 MTJ system, and found its TMR can be controlled from 17,000% to 57,000% [189]. Another comparable work combining voltage control was done by Jiang *et al*. [190]. A TMR up to 1,000,000% at 1.4 K under a 2 T magnetic field was also reported by Kim *et al*. [186] using multilayer CrI_3.

But a main disadvantage of CrI_3-based devices is that the operating temperature is far too lower than room temperature. By comparison, Fe_3GeTe_2 has a higher T_C, which is more conducive to be promoted to practical applications. The constructed Fe_3GeTe_2/hBN/Fe_3GeTe_2 heterostructure is found to have a TMR up to 160%, revealed by low-temperature anomalous Hall effect measurements [6]. There are also some theoretical works demonstrating this MTJ system [191,192]. By substituting the hBN barrier to other materials like graphite or

MoS_2, different phenomena emerge. A strong spin-obit coupling can be observed in the Fe_3GeTe_2/graphite interface [193], while the MoS_2 acts as a conductor layer in the MTJ with a TMR of 3.1% [194]. The switching and tuning of MTJs at present are mainly realized by applying an external magnetic field, which is currently a main limitation for future applications. All-electric switching would be achieved by methods of spin transfer torque (STT) and spin orbit torque (SOT) [195], and SOT can be put forward to integrate SOT-MRAM [196–198].

Challenges and outlooks for spin-phonon coupling investigation in 2DMMs

Along with the development of 2DMM, the investigations related to spin-phonon coupling have contributed to understanding 2D magnetism, mediating magnetism and improving device functionalities. In this field, we believe that there are still several directions to be pursued in both fundamental study and potential applications of 2DMMs. We have listed a mass of van der Waals magnetic materials in Table 1 when we discussed synthesis contents, while only few of them were well studied on their exfoliated counterparts as well as their magnetic behaviors. We can find that those unexplored van der Waals magnets are spread out across many types, including perovskite with strong luminescence, topological insulators, multiferroic materials, quantum spin liquids, and superconductors. As a general effect in magnetic materials, spin-phonon coupling has great potential to couple with various (quasi-)particles in condensed matter and exhibits new physical features. Finding new types of spin-phonon couplings is not only the focus of physics research in 2D materials but also essential to the investigation of new phases and regulation of physical states. Besides that, as an intrinsic property of the electron, charge is found to intertwine tightly with both spin and phonon in 2DMMs, while the underlying mechanism is still unclear. More theoretical and experimental investigations are needed to help us understand the critical function of charge in spin-phonon coupling.

Moreover, most current spin-phonon coupling investigations are in equilibrium. However, how the phonon behaves during the spin-wave propagation or how the spin behaved during the phonon excitation is understood inadequately. To understand the dynamic spin-phonon coupling effect in 2DMM, ultra-fast optical methods can play an important role. Using intense mid-infrared electric field pulses which are resonant with a phonon mode of magnetic materials, those light-generated phonons can be utilized to coherently manipulate macroscopic magnetic states in 3D magnets. It has been realized experimentally in 3D perovskite magnetic insulator $DyFeO_3$, where resonant phonon excitation induces ultrafast and long-lived changes in the exchange interactions between rare-earth orbitals and transition metal spins [199]. The optical tuning strategy can be extended to 2D systems, where important explorations are made on few 2DMMs, including CoF_2 [45] and $NiPS_3$ [115,159]. In addition to using mid-infrared or terahertz light to directly excite one or several phonon modes, terahertz light can also be used to excite electrons and then indirectly excite phonon modes and magnon modes through electron-phonon coupling and spin-charge coupling, respectively. The corresponding research is still in its infancy [200].

Utilizing the ubiquitous spin-phonon coupling in 2DMMs, 2DMM-based spintronic and magnonic devices can be developed. Magnetic materials are the key constituent in information storage devices. The speed of data storage is related to the transformation speed between different magnetic states. At present, the speed of data storage is mainly at the GHz level [201,202]. Using phonon excitation to tune the magnetism through

spin-phonon coupling has become a potential approach to improve the data read/write speed. Another obstacle preventing the application of 2DMMs is the low magnetic transition temperature. In the current stage, most of the demonstrations of 2DMM-based spintronic or magnonic devices are conducted at temperatures far below room temperature. Based on spin-phonon coupling, the magnetic anisotropy can be enhanced and the magnetic phase transition temperature can be achieved. Pioneering studies have been done in recent years. Liu *et al*. [203] integrated Mn_3Pt with piezoelectric substrate $BaTiO_3$ and utilized the electric field tuned interface strain to tune the topological anomalous Hall effect in the heterostructure. In addition, by driving specific phonon modes optically, the magnetic anisotropy can be enhanced, thus the magnetic transition temperature can be extensively raised, where the THz optical pulses might find their abilities.

Compared with the case in 3D magnetic materials, realizing "read" and "write" in 2DMMs might encounter more difficulties. 2DMMs with nanoscale thickness usually have much smaller sizes compared with 3D materials, resulting in much smaller optical/electronic signals. Precise magnetic detection and effective spin control require more sophisticated methods. Designing techniques based on brand-new physical mechanisms may be another efficient way to solve this dilemma in 2DMMs. At present, the 2D magnetic materials and their heterostructures are still mainly in the stage of fundamental physics research, and the preparation of high-quality samples mostly depends on mechanical exfoliation and transfer, which are difficult to be promoted to large-scale device fabrication. Based on the existing research, the main challenges in promoting 2D magnetic materials to wider applications in the future include finding materials with higher phase transition temperature and better stability in ambient conditions, optimizing the preparation process and method, accessing lower energy consumption, etc. Moreover, since the spin-phonon coupling effect is one of the main channels for spin decoherence in qubit, how to tune the strength of spin-phonon coupling effect itself in 2DMMs also needs to be explored. In this young and rapidly developing field, we look forward to more exciting breakthroughs in the future.

Funding

Q.X gratefully acknowledges the strong funding support from the National Natural Science Foundation of China (12250710126), strong support from the State Key Laboratory of Low-Dimensional Quantum Physics, and funding support by Tsinghua University Initiative Scientific Research Programfrom and startup grant from Tsinghua University. X.W. acknowledges the support by the National Key R&D Program of China (2022YFA1602704), the National Natural Science Foundation of China (62275225), and the Fundamental Research Funds for the Central Universities (20720220034).

Conflict of interest

The authors declare no conflict of interest.

References

1 Žutić I, Fabian J, Das Sarma S. Spintronics: Fundamentals and applications. *Rev Mod Phys* 2004; **76**: 323–410.

2 Yuan HY, Cao Y, Kamra A, *et al.* Quantum magnonics: When magnon spintronics meets quantum information science. *Phys Rep* 2022; **965**: 1–74.

3 Kasahara Y, Ohnishi T, Mizukami Y, *et al.* Majorana quantization and half-integer thermal quantum Hall effect in a Kitaev spin liquid. *Nature* 2018; **559**: 227–231.

4 Gong C, Zhang X. Two-dimensional magnetic crystals and emergent heterostructure devices. *Science* 2019; **363**: eaav4450.

5 Wang Z, Gutiérrez-Lezama I, Ubrig N, *et al.* Very large tunneling magnetoresistance in layered magnetic semiconductor CrI_3. *Nat Commun* 2018; **9**: 2516.

6 Wang Z, Sapkota D, Taniguchi T, *et al.* Tunneling spin valves based on Fe_3GeTe_2/hBN/Fe_3GeTe_2 van der Waals heterostructures. *Nano Lett* 2018; **18**: 4303–4308.

7 Kezilebieke S, Huda MN, Vaňo V, *et al.* Topological superconductivity in a van der Waals heterostructure. *Nature* 2020; **588**: 424–428.

8 Souchkov AB, Simpson JR, Quijada M, *et al.* Exchange interaction effects on the optical properties of $LuMnO_3$. *Phys Rev Lett* 2003; **91**: 027203.

9 Mochizuki M, Furukawa N, Nagaosa N. Theory of spin-phonon coupling in multiferroic manganese perovskites $RMnO_3$. *Phys Rev B* 2011; **84**: 144409.

10 Sivadas N, Okamoto S, Xu X, *et al.* Stacking-dependent magnetism in bilayer CrI_3. *Nano Lett* 2018; **18**: 7658–7664.

11 Webster L, Liang L, Yan JA. Distinct spin-lattice and spin-phonon interactions in monolayer magnetic CrI_3. *Phys Chem Chem Phys* 2018; **20**: 23546–23555.

12 Wang X, Du K, Fredrik Liu YY, *et al.* Raman spectroscopy of atomically thin two-dimensional magnetic iron phosphorus trisulfide ($FePS_3$) crystals. *2D Mater* 2016; **3**: 031009.

13 Sun YJ, Tan QH, Liu XL, *et al.* Probing the magnetic ordering of antiferromagnetic $MnPS_3$ by Raman spectroscopy. *J Phys Chem Lett* 2019; **10**: 3087–3093.

14 Hu X, Zhao Y, Shen X, *et al.* Enhanced ferromagnetism and tunable magnetism in Fe_3GeTe_2 monolayer by strain engineering. *ACS Appl Mater Interfaces* 2020; **12**: 26367–26373.

15 Qing X, Li H, Zhong C, *et al.* Magnetism and spin exchange coupling in strained monolayer CrOCl. *Phys Chem Chem Phys* 2020; **22**: 17255–17262.

16 Go G, Kim SK, Lee KJ. Topological magnon-phonon hybrid excitations in two-dimensional ferromagnets with tunable chern numbers. *Phys Rev Lett* 2019; **123**: 237207.

17 Zhang BH, Hou YS, Wang Z, *et al.* First-principles studies of spin-phonon coupling in monolayer $Cr_2Ge_2Te_6$. *Phys Rev B* 2019; **100**: 224427.

18 Huang B, Cenker J, Zhang X, *et al.* Tuning inelastic light scattering via symmetry control in the two-dimensional magnet CrI_3. *Nat Nanotechnol* 2020; **15**: 212–216.

19 Liu S, Granados del Águila A, Bhowmick D, *et al.* Direct observation of magnon-phonon strong coupling in two-dimensional antiferromagnet at high magnetic fields. *Phys Rev Lett* 2021; **127**: 097401.

20 Li T, Jiang S, Sivadas N, *et al.* Pressure-controlled interlayer magnetism in atomically thin CrI_3. *Nat Mater* 2019; **18**: 1303–1308.

21 Cenker J, Sivakumar S, Xie K, *et al.* Reversible strain-induced magnetic phase transition in a van der Waals magnet. *Nat Nanotechnol* 2022; **17**: 256–261.

22 Baltz V, Manchon A, Tsoi M, *et al.* Antiferromagnetic spintronics. *Rev Mod Phys* 2018; **90**: 015005.

23 Mirzoyan R, Hadt RG. The dynamic ligand field of a molecular qubit: Decoherence through spin-phonon coupling. *Phys Chem Chem Phys* 2020; **22**: 11249–11265.

24 Maehrlein SF, Radu I, Maldonado P, *et al.* Dissecting spin-phonon equilibration in ferrimagnetic insulators by ultrafast lattice excitation. *Sci Adv* 2018; **4**: eaar5164.

25 Mermin ND, Wagner H. Absence of ferromagnetism or antiferromagnetism in one- or two-dimensional isotropic heisenberg models. *Phys Rev Lett* 1966; **17**: 1133–1136.

26 Huang B, Clark G, Navarro-Moratalla E, *et al.* Layer-dependent ferromagnetism in a van der Waals crystal down to the monolayer limit. *Nature* 2017; **546**: 270–273.

27 Gong C, Li L, Li Z, *et al.* Discovery of intrinsic ferromagnetism in two-dimensional van der Waals crystals. *Nature* 2017; **546**: 265–269.

28 Burch KS, Mandrus D, Park JG. Magnetism in two-dimensional van der Waals materials. *Nature* 2018; **563**: 47–52.

29 Tian Y, Gray MJ, Ji H, *et al.* Magneto-elastic coupling in a potential ferromagnetic 2D atomic crystal. *2D Mater* 2016;

3: 025035.

30 Lee JU, Lee S, Ryoo JH, *et al.* Ising-type magnetic ordering in atomically thin $FePS_3$. *Nano Lett* 2016; **16**: 7433–7438.

31 Du L, Tang J, Zhao Y, *et al.* Lattice dynamics, phonon chirality, and spin-phonon coupling in 2D itinerant ferromagnet Fe_3GeTe_2. *Adv Funct Mater* 2019; **29**: 1904734.

32 Lyu BB, Gao YF, Zhang Y, *et al.* Probing the ferromagnetism and spin wave gap in VI_3 by helicity-resolved Raman spectroscopy. *Nano Lett* 2020; **20**: 6024–6031.

33 Yin T, Ulman KA, Liu S, *et al.* Chiral phonons and giant magneto-optical effect in $CrBr_3$ 2D magnet. *Adv Mater* 2021; **33**: 2101618.

34 Kozlenko DP, Lis ON, Kichanov SE, *et al.* Spin-induced negative thermal expansion and spin-phonon coupling in van der Waals material $CrBr_3$. *npj Quantum Mater* 2021; **6**: 19.

35 López-Paz SA, Guguchia Z, Pomjakushin VY, *et al.* Dynamic magnetic crossover at the origin of the hidden-order in van der Waals antiferromagnet CrSBr. *Nat Commun* 2022; **13**: 4745.

36 Gu P, Sun Y, Wang C, *et al.* Magnetic phase transitions and magnetoelastic coupling in a two-dimensional stripy antiferromagnet. *Nano Lett* 2022; **22**: 1233–1241.

37 Hentrich R, Wolter AU , Zotos X, *et al.* Unusual phonon heat transport in α-$RuCl_3$: Strong spin-phonon scattering and field-induced spin gap. *Phys Rev Lett* 2018; **120**: 117204.

38 Choe J, Lujan D, Rodriguez-Vega M, *et al.* Electron-phonon and spin-lattice coupling in atomically thin layers of $MnBi_2Te_4$. *Nano Lett* 2021; **21**: 6139–6145.

39 Chen W, Sun Z, Wang Z, *et al.* Direct observation of van der Waals stacking-dependent interlayer magnetism. *Science* 2019; **366**: 983–987.

40 Ni Z, Haglund AV, Wang H, *et al.* Imaging the Néel vector switching in the monolayer antiferromagnet $MnPSe_3$ with strain-controlled Ising order. *Nat Nanotechnol* 2021; **16**: 782–787.

41 Du K, Wang X, Liu Y, *et al.* Weak van der Waals stacking, wide-range band gap, and Raman study on ultrathin layers of metal phosphorus trichalcogenides. *ACS Nano* 2016; **10**: 1738–1743.

42 Wang Y, Ying J, Zhou Z, *et al.* Emergent superconductivity in an iron-based honeycomb lattice initiated by pressure-driven spin-crossover. *Nat Commun* 2018; **9**: 1914.

43 Bonilla M, Kolekar S, Ma Y, *et al.* Strong room-temperature ferromagnetism in VSe_2 monolayers on van der Waals substrates. *Nat Nanotech* 2018; **13**: 289–293.

44 Song T, Fei Z, Yankowitz M, *et al.* Switching 2D magnetic states via pressure tuning of layer stacking. *Nat Mater* 2019; **18**: 1298–1302.

45 Disa AS, Fechner M, Nova TF, *et al.* Polarizing an antiferromagnet by optical engineering of the crystal field. *Nat Phys* 2020; **16**: 937–941.

46 Jiang S, Xie H, Shan J, *et al.* Exchange magnetostriction in two-dimensional antiferromagnets. *Nat Mater* 2020; **19**: 1295–1299.

47 Song T, Sun QC, Anderson E, *et al.* Direct visualization of magnetic domains and Moiré magnetism in twisted 2D magnets. *Science* 2021; **374**: 1140–1144.

48 Du K, Tu Q, Zhang X, *et al.* Two-dimensional lead(II) halide-based hybrid perovskites templated by acene alkylamines: Crystal structures, optical properties, and piezoelectricity. *Inorg Chem* 2017; **56**: 9291–9302.

49 Sun B, Liu XF, Li XY, *et al.* Reversible thermochromism and strong ferromagnetism in two-dimensional hybrid perovskites. *Angew Chem Int Ed* 2020; **59**: 203–208.

50 Polyakov AO, Arkenbout AH, Baas J, *et al.* Coexisting ferromagnetic and ferroelectric order in a $CuCl_4$-based organic-inorganic hybrid. *Chem Mater* 2012; **24**: 133–139.

51 Willett R, Place H, Middleton M. Crystal structures of three new copper(II) halide layered perovskites: Structural, crystallographic, and magnetic correlations. *J Am Chem Soc* 1988; **110**: 8639–8650.

52 Ai Y, Sun R, Liao W-, *et al.* Unprecedented ferroelectricity and ferromagnetism in a Cr^{2+}-based two-dimensional hybrid perovskite. *Angew Chem Int Ed* 2022; **61**: .

53 Stead MJ, Day P. Preparation, characterization, and magnetic properties of organic-intercalated two-dimensional ionic ferromagnets $(C_nH_{2n+1}NH_3)_2CrCl_4$ (n = 3, 5, or 12). *J Chem Soc Dalton Trans* 1982; 1081, https://doi/org/10.1039/DT9820001081.

54 Yaffe O, Chernikov A, Norman ZM, *et al.* Excitons in ultrathin organic-inorganic perovskite crystals. *Phys Rev B* 2015; **92**: 045414.

55 Wang N, Tang H, Shi M, *et al.* Transition from ferromagnetic semiconductor to ferromagnetic metal with enhanced curie temperature in $Cr_2Ge_2Te_6$ via organic ion intercalation. *J Am Chem Soc* 2019; **141**: 17166–17173.

56 Carteaux V, Ouvrard G, Grenier JC, *et al.* Magnetic structure of the new layered ferromagnetic chromium hexatellurosilicate $Cr_2Si_2Te_6$. *J Magn Magn Mater* 1991; **94**: 127–133.

57 Chen B, Yang JH, Wang HD, *et al.* Magnetic properties of layered itinerant electron ferromagnet Fe_3GeTe_2. *J Phys Soc Jpn* 2013; **82**: 124711.

58 Nikonov KS, Brekhovskikh MN, Egorysheva AV, *et al.* Chemical vapor transport growth of vanadium(IV) selenide and vanadium(IV) telluride single crystals. *Inorg Mater* 2017; **53**: 1126–1130.

59 Schmidt M, Gooth J, Binnewies M. Preparation and crystal growth of transition metal dichalcogenides. *Z Anorg Allg Chem* 2020; **646**: 1183–1194.

60 Jin W, Kim HH, Ye Z, *et al.* Raman fingerprint of two terahertz spin wave branches in a two-dimensional honeycomb Ising ferromagnet. *Nat Commun* 2018; **9**: 5122.

61 Pan S, Bai Y, Tang J, *et al.* Growth of high-quality CrI_3 single crystals and engineering of its magnetic properties via V and Mn doping. *J Alloys Compd* 2022; **908**: 164573.

62 Ahn K, Felser C, Seshadri R, *et al.* Giant negative magnetoresistance in GdI_2. *J Alloys Compd* 2000; **303-304**: 252–256.

63 Tian S, Zhang JF, Li C, *et al.* Ferromagnetic van der Waals Crystal VI_3. *J Am Chem Soc* 2019; **141**: 5326–5333.

64 Binnewies M, Glaum R, Schmidt M, Schmidt P. *Chemical Vapor Transport Reactions*. Berlin: Walter de Gruyter, 2012.

65 Kinomura N, Terao K, Kikkawa S, *et al.* Synthesis and crystal structure of InP_3. *Mater Res Bull* 1983; **18**: 53–57.

66 Zhu C, Lei Z, Song L, *et al.* Synthesis and growth of GaSe single crystals. *J Cryst Growth* 2015; **421**: 53–57.

67 Attolini G, Negri M, Besagni T, *et al.* CVT and PVT growth and characterization of GaS crystals. *Mater Sci Eng-B* 2020; **261**: 114623.

68 Yamamoto N, Endo T, Shimada M, *et al.* Single crystal growth of α-MnO_2. *Jpn J Appl Phys* 1974; **13**: 723–724.

69 Yan JQ, Sales BC, Susner MA, *et al.* Flux growth in a horizontal configuration: An analog to vapor transport growth. *Phys Rev Mater* 2017; **1**: 023402.

70 Park CB, Shahee A, Kim KT, *et al.* Observation of spin-induced ferroelectricity in a layered van der Waals antiferromagnet $CuCrP_2S_6$. *Adv Elect Mater* 2022; **8**: 2101072.

71 Selter S, Shemerliuk Y, Büchner B, *et al.* Crystal growth of the quasi-2D quarternary compound $AgCrP_2S_6$ by chemical vapor transport. *Crystals* 2021; **11**: 500.

72 Lee S, Colombet P, Ouvrard G, *et al.* A new chain compound of vanadium (III): Structure, metal ordering, and magnetic properties. *Mater Res Bull* 1986; **21**: 917–928.

73 van Bruggen CF, Haange RJ, Wiegers GA, *et al.* $CrSe_2$, a new layered dichalcogenide. *Physica B+C* 1980; **99**: 166–172.

74 Freitas DC, Weht R, Sulpice A, *et al.* Ferromagnetism in layered metastable 1 *T*-$CrTe_2$. *J Phys-Condens Matter* 2015; **27**: 176002.

75 McGuire MA, Garlea VO, Kc S, *et al.* Antiferromagnetism in the van der Waals layered spin-lozenge semiconductor $CrTe_3$. *Phys Rev B* 2017; **95**: 144421.

76 McGuire MA, DiSalvo FJ. $Ni_3Cr_2P_2Q_9$ (Q = S, Se): New quaternary transition metal chalcogenides with a unique layered structure. *Chem Mater* 2007; **19**: 4600–4605.

77 Yan JQ, Huang Z, Wu W, *et al.* Vapor transport growth of $MnBi_2Te_4$ and related compounds. *J Alloys Compd* 2022; **906**: 164327.

78 Nowka C, Gellesch M, Enrique Hamann Borrero J, *et al.* Chemical vapor transport and characterization of $MnBi_2Se_4$. *J Cryst Growth* 2017; **459**: 81–86.

79 Kim HH, Yang B, Li S, *et al.* Evolution of interlayer and intralayer magnetism in three atomically thin chromium trihalides. *Proc Natl Acad Sci USA* 2019; **116**: 11131–11136.

80 Haberecht J, Borrmann H, Kniep R. Refinement of the crystal structure of iron dibromide, $FeBr_2$. *Z für Kristallographie-New Cryst Struct* 2001; **216**: 544.

81 Coleman CC, Yamada E. Optimization of the vapor reaction growth of single crystal FeI_2. *J Cryst Growth* 1993; **132**: 129–133.

82 McCarley RE, Roddy JW, Berry KO. Transport reactions of some vanadium(III) halides. Mixed halide formation. *Inorg Chem* 1964; **3**: 50–54.

83 Hashimoto S, Forster K, Moss SC. Structure refinement of an $FeCl_3$ crystal using a thin plate sample. *J Appl Crystlogr* 1989; **22**: 173–180.

84 Armbruster M, Rotter HW, Thiele G. ChemInform abstract: Preparation and spectroscopic characterization of strontium and barium tetrabromoferrate(III) and the crystal structure of $Ba(FeBr_4)_2$. *ChemInform* 2000; **31**: no.

85 Zeng Y, Gu P, Zhao Z, *et al.* 2D FeOCl: A highly in-plane anisotropic antiferromagnetic semiconductor synthesized via temperature-oscillation chemical vapor transport. *Adv Mater* 2022; **34**: 2108847.

86 Wang W, Sun R, He S, *et al.* Atomic structure, work function and magnetism in layered single crystal VOCl. *2D Mater* 2020; **8**: 015027.

87 Klein J, Pham T, Thomsen JD, *et al.* Control of structure and spin texture in the van der Waals layered magnet CrSBr. *Nat Commun* 2022; **13**: 5420.

88 Kong T, Guo S, Ni D, *et al.* Crystal structure and magnetic properties of the layered van der Waals compound VBr_3. *Phys Rev Mater* 2019; **3**: 084419.

89 Han J, Nishihara S, Inoue K, *et al.* On the nature of the structural and magnetic phase transitions in the layered perovskite-like $(CH_3NH_3)_2[Fe^{II}Cl_4]$. *Inorg Chem* 2014; **53**: 2068–2075.

90 Han J, Nishihara S, Inoue K, *et al.* High magnetic hardness for the canted antiferromagnetic, ferroelectric, and ferroelastic layered perovskite-like $(C_2H_5NH_3)_2[Fe^{II}\ Cl_4]$. *Inorg Chem* 2015; **54**: 2866–2874.

91 Septiany L, Tulip D, Chislov M, *et al.* Polar structure and two-dimensional heisenberg antiferromagnetic properties of arylamine-based manganese chloride layered organic-inorganic perovskites. *Inorg Chem* 2021; **60**: 15151–15158.

92 Oeckler O, Simon A. Redetermination of the crystal structure of copper dibromide, $CuBr_2$. *Z für Kristallographie-New Cryst Struct* 2000; **215**: 13.

93 Kuindersma SR, Sanchez JP, Haas C. Magnetic and structural investigations on NiI_2 and CoI_2. *Physica B+C* 1981; **111**: 231–248.

94 Li Y, Chen D, Dong X, *et al.* Magnetic and electric properties of single crystal MnI_2. *J Phys-Condens Matter* 2020; **32**: 335803.

95 Guo YQ, Tan RQ, Li X, *et al.* Shape-controlled growth and single-crystal XRD study of submillimeter-sized single crystals of SnO. *CrystEngComm* 2011; **13**: 5677.

96 Solanki GK, Patel DB, Unadkat S, *et al.* Synthesis and characterization of germanium monosulphide (GeS) single crystals grown using different transporting agents. *Pramana* 2010; **74**: 813–825.

97 Wiedemeier H, Irene EA, Chaudhuri AK. Crystal growth by vapor transport of GeSe, $GeSe_2$, and GeTe and transport mechanism and morphology of GeTe. *J Cryst Growth* 1972; **13-14**: 393–396.

98 Burton LA, Colombara D, Abellon RD, *et al.* Synthesis, characterization, and electronic structure of single-crystal SnS, Sn_2S_3, and SnS_2. *Chem Mater* 2013; **25**: 4908–4916.

99 Patel S, Chaki SH, Vinodkumar PC. Pure SnSe, In and Sb doped SnSe single crystals – Growth, structural, surface morphology and optical bandgap study. *J Cryst Growth* 2019; **522**: 16–24.

100 Hahn H, Katscher H. Über chalkogenidhalogenide des galliums. *Z Anorg Allg Chem* 1963; **321**: 85–93.

101 Aoki M, Yamane H, Shimada M, *et al.* CrN single-crystal growth using Cr-Ga-Na ternary melt. *J Cryst Growth* 2002;

246: 133–138.

102 Okada S, Kudou K, Iizumi K, *et al.* Single-crystal growth and properties of CrB, Cr_3B_4, Cr_2B_3 and CrB_2 from high-temperature aluminum solutions. *J Cryst Growth* 1996; **166**: 429–435.

103 Hyde KR, Hooper EW, Waters J, *et al.* α- and β-ruthenium trichloride. *J Less Common Met* 1965; **8**: 428–434.

104 Hepworth MA, Jack KH. The crystal structure of manganese trifluoride, MnF_3. *Acta Cryst* 1957; **10**: 345–351.

105 Schäfer H, Wartenpfuhl F, Weise E. Über Titanchloride. V. Titan(III)-oxychlorid. *Zeitschrift für anorganische und allgemeine Chemie*, 1958, 295: 268–280.

106 Schnering HGV, Collin M, Hassheider M. TiOBr, darstellung, eigenschaften und struktur. *Zeitschrift für Anorganische und Allgemeine Chemie*, 1972, 387: 137–141.

107 Huang B, McGuire MA, May AF, *et al.* Emergent phenomena and proximity effects in two-dimensional magnets and heterostructures. *Nat Mater* 2020; **19**: 1276–1289.

108 Zhai B, Du J, Li X, *et al.* Two-dimensional ferromagnetic materials and related van der Waals heterostructures: A first-principle study. *J Semicond* 2019; **40**: 081509.

109 Zhang J, Yang J, Lin L, *et al.* An antiferromagnetic two-dimensional material: Chromium diiodides monolayer. *J Semicond* 2020; **41**: 122502.

110 Zhang WB, Qu Q, Zhu P, *et al.* Robust intrinsic ferromagnetism and half semiconductivity in stable two-dimensional single-layer chromium trihalides. *J Mater Chem C* 2015; **3**: 12457–12468.

111 Deng Y, Yu Y, Song Y, *et al.* Gate-tunable room-temperature ferromagnetism in two-dimensional Fe_3GeTe_2. *Nature* 2018; **563**: 94–99.

112 Dirnberger F, Bushati R, Datta B, *et al.* Spin-correlated exciton–polaritons in a van der Waals magnet. *Nat Nanotechnol* 2022; **17**: 1060–1064.

113 Xu Y, Ray A, Shao YT, *et al.* Coexisting ferromagnetic-antiferromagnetic state in twisted bilayer CrI_3. *Nat Nanotechnol* 2022; **17**: 143–147.

114 Wang X, Cao J, Li H, *et al.* Electronic Raman scattering in the 2D antiferromagnet $NiPS_3$. *Sci Adv* 2022; **8**: eabl7707.

115 Afanasiev D, Hortensius JR, Matthiesen M, *et al.* Controlling the anisotropy of a van der Waals antiferromagnet with light. *Sci Adv* 2021; **7**: eabf3096.

116 Song T, Cai X, Tu MWY, *et al.* Giant tunneling magnetoresistance in spin-filter van der Waals heterostructures. *Science* 2018; **360**: 1214–1218.

117 Webster L, Yan JA. Strain-tunable magnetic anisotropy in monolayer $CrCl_3$, $CrBr_3$, and CrI_3. *Phys Rev B* 2018; **98**: 144411.

118 McGuire M. Crystal and magnetic structures in layered, transition metal dihalides and trihalides. *Crystals* 2017; **7**: 121.

119 McGuire MA, Dixit H, Cooper VR, *et al.* Coupling of crystal structure and magnetism in the layered, ferromagnetic insulator CrI_3. *Chem Mater* 2015; **27**: 612–620.

120 Jiang X, Liu Q, Xing J, *et al.* Recent progress on 2D magnets: Fundamental mechanism, structural design and modification. *Appl Phys Rev* 2021; **8**: 031305.

121 Zhang Y, Wu X, Lyu BB, *et al.* Magnetic order-induced polarization anomaly of Raman scattering in 2D magnet CrI_3. *Nano Lett* 2020; **20**: 729–734.

122 Thingstad E, Kamra A, Brataas A, *et al.* Chiral phonon transport induced by topological magnons. *Phys Rev Lett* 2019; **122**: 107201.

123 Sheikhi B, Kargarian M, Langari A. Hybrid topological magnon-phonon modes in ferromagnetic honeycomb and kagome lattices. *Phys Rev B* 2021; **104**: 045139.

124 Rahman S, Torres JF, Khan AR, *et al.* Recent developments in van der Waals antiferromagnetic 2D materials: Synthesis, characterization, and device implementation. *ACS Nano* 2021; **15**: 17175–17213.

125 Mai TT, Garrity KF, McCreary A, *et al.* Magnon-phonon hybridization in 2D antiferromagnet $MnPSe_3$. *Sci Adv* 2021; **7**: eabj3106.

126 Kim K, Lim SY, Lee JU, *et al.* Suppression of magnetic ordering in XXZ-type antiferromagnetic monolayer $NiPS_3$. *Nat*

Commun 2019; **10**: 345.

127 Kang S, Kim K, Kim BH, *et al.* Coherent many-body exciton in van der Waals antiferromagnet $NiPS_3$. *Nature* 2020; **583**: 785–789.

128 Wang X, Cao J, Lu Z, *et al.* Spin-induced linear polarization of photoluminescence in antiferromagnetic van der Waals crystals. *Nat Mater* 2021; **20**: 964–970.

129 Hwangbo K, Zhang Q, Jiang Q, *et al.* Highly anisotropic excitons and multiple phonon bound states in a van der Waals antiferromagnetic insulator. *Nat Nanotechnol* 2021; **16**: 655–660.

130 Zhang S, Xu R, Luo N, *et al.* Two-dimensional magnetic materials: Structures, properties and external controls. *Nanoscale* 2021; **13**: 1398–1424.

131 Lee K, Dismukes AH, Telford EJ, *et al.* Magnetic order and symmetry in the 2D semiconductor CrSBr. *Nano Lett* 2021; **21**: 3511–3517.

132 Zhang T, Wang Y, Li H, *et al.* Magnetism and optical anisotropy in van der Waals antiferromagnetic insulator CrOCl. *ACS Nano* 2019; **13**: 11353–11362.

133 Pawbake A, Pelini T, Wilson NP, *et al*. Raman scattering signatures of the strong spin-phonon coupling in the bulk magnetic van der Waals material CrSBr. arXiv preprint, arxiv: 2211.12939, 2022.

134 Angelkort J, Wölfel A, Schönleber A, *et al.* Observation of strong magnetoelastic coupling in a first-order phase transition of CrOCl. *Phys Rev B* 2009; **80**: 144416.

135 Wang WJ, Xu XT, Shen J, *et al.* Spin-phonon coupling in van der Waals antiferromagnet VOCl. *Chin Phys B* 2021; **30**: 107502.

136 Fei Z, Huang B, Malinowski P, *et al.* Two-dimensional itinerant ferromagnetism in atomically thin Fe_3GeTe_2. *Nat Mater* 2018; **17**: 778–782.

137 Zhang L, Song L, Dai H, *et al.* Substrate-modulated ferromagnetism of two-dimensional Fe_3GeTe_2. *Appl Phys Lett* 2020; **116**: 042402.

138 Zhu W, Song C, Han L, *et al.* van der Waals lattice-induced colossal magnetoresistance in $Cr_2Ge_2Te_6$ thin flakes. *Nat Commun* 2022; **13**: 6428.

139 Sivadas N, Daniels MW, Swendsen RH, *et al.* Magnetic ground state of semiconducting transition-metal trichalcogenide monolayers. *Phys Rev B* 2015; **91**: 235425.

140 Pei Q, Wang XC, Zou JJ, *et al.* Tunable electronic structure and magnetic coupling in strained two-dimensional semiconductor $MnPSe_3$. *Front Phys* 2018; **13**: 137105.

141 Wu J, Yao Y, Lin ML, *et al.* Spin-phonon coupling in ferromagnetic monolayer chromium tribromide. *Adv Mater* 2022; **34**: 2108506.

142 Pandey T, Peeters FM, Milošević MV. Pivotal role of magnetic ordering and strain in lattice thermal conductivity of chromium-trihalide monolayers. *2D Mater* 2022; **9**: 015034.

143 Liu Y, Liu Q, Liu Y, *et al.* Effects of spin-phonon coupling on two-dimensional ferromagnetic semiconductors: A case study of iron and ruthenium trihalides. *Nanoscale* 2021; **13**: 7714–7722.

144 Sun YJ, Pang SM, Zhang J. Review of Raman spectroscopy of two-dimensional magnetic van der Waals materials. *Chin Phys B* 2021; **30**: 117104.

145 Padmanabhan H, Poore M, Kim PK, *et al.* Interlayer magnetophononic coupling in $MnBi_2Te_4$. *Nat Commun* 2022; **13**: 1929.

146 Sun YJ, Lai JM, Pang SM, *et al.* Magneto-Raman study of magnon-phonon coupling in two-dimensional ising antiferromagnetic $FePS_3$. *J Phys Chem Lett* 2022; **13**: 1533–1539.

147 Liu Z, Guo K, Hu G, *et al.* Observation of nonreciprocal magnetophonon effect in nonencapsulated few-layered CrI_3. *Sci Adv* 2020; **6**: eabc7628.

148 Jin W, Ye Z, Luo X, *et al.* Tunable layered-magnetism-assisted magneto-Raman effect in a two-dimensional magnet CrI_3. *Proc Natl Acad Sci USA* 2020; **117**: 24664–24669.

149 McCreary A, Mai TT, Utermohlen FG, *et al.* Distinct magneto-Raman signatures of spin-flip phase transitions in CrI_3.

Nat Commun 2020; **11**: 3879.

150 Vaclavkova D, Palit M, Wyzula J, *et al.* Magnon polarons in the van der Waals antiferromagnet $FePS_3$. *Phys Rev B* 2021; **104**: 134437.

151 Ghosh A, Palit M, Maity S, *et al.* Spin-phonon coupling and magnon scattering in few-layer antiferromagnetic $FePS_3$. *Phys Rev B* 2021; **103**: 064431.

152 Webster L, Liang L, Yan JA. Correction: Distinct spin-lattice and spin-phonon interactions in monolayer magnetic CrI_3. *Phys Chem Chem Phys* 2022; **24**: 17898.

153 Shin D, Hübener H, De Giovannini U, *et al.* Phonon-driven spin-floquet magneto-valleytronics in MoS_2. *Nat Commun* 2018; **9**: 638.

154 He J, Frauenheim T. Optically driven ultrafast magnetic order transitions in two-dimensional ferrimagnetic MXenes. *J Phys Chem Lett* 2020; **11**: 6219–6226.

155 Belvin CA, Baldini E, Ozel IO, *et al.* Exciton-driven antiferromagnetic metal in a correlated van der Waals insulator. *Nat Commun* 2021; **12**: 4837.

156 Zhang XX, Jiang S, Lee J, *et al.* Spin dynamics slowdown near the antiferromagnetic critical point in atomically thin $FePS_3$. *Nano Lett* 2021; **21**: 5045–5052.

157 Bae YJ, Wang J, Scheie A, *et al.* Exciton-coupled coherent magnons in a 2D semiconductor. *Nature* 2022; **609**: 282–286.

158 Bartram FM, Leng YC, Wang Y, *et al.* Ultrafast coherent interlayer phonon dynamics in atomically thin layers of $MnBi_2Te_4$. *npj Quantum Mater* 2022; **7**: 84.

159 Ergeçen E, Ilyas B, Mao D, *et al.* Magnetically brightened dark electron-phonon bound states in a van der Waals antiferromagnet. *Nat Commun* 2022; **13**: 98.

160 Gong Y, Hu M, Harris N, *et al.* Strong laser polarization control of coherent phonon excitation in van der Waals material Fe_3GeTe_2. *npj 2D Mater Appl* 2022; **6**: 9.

161 Padmanabhan P, Buessen FL, Tutchton R, *et al.* Coherent helicity-dependent spin-phonon oscillations in the ferromagnetic van der Waals crystal CrI_3. *Nat Commun* 2022; **13**: 4473.

162 Chumak AV, Vasyuchka VI, Serga AA, *et al.* Magnon spintronics. *Nat Phys* 2015; **11**: 453–461.

163 Kruglyak VV, Demokritov SO, Grundler D. Magnonics. *J Phys D-Appl Phys* 2010; **43**: 264001.

164 Mertens F, Mönkebüscher D, Parlak U, *et al.* Ultrafast coherent THz lattice dynamics coupled to spins in the van der Waals antiferromagnet $FePS_3$. *Adv Mater* 2023; **35**: 2208355.

165 Kim SY, Kim TY, Sandilands LJ, *et al.* Charge-spin correlation in van der Waals antiferromagnet $NiPS_3$. *Phys Rev Lett* 2018; **120**: 136402.

166 Deng Y, Yu Y, Shi MZ, *et al.* Quantum anomalous Hall effect in intrinsic magnetic topological insulator $MnBi_2Te_4$. *Science* 2020; **367**: 895–900.

167 Coak MJ, Jarvis DM, Hamidov H, *et al.* Emergent magnetic phases in pressure-tuned van der Waals antiferromagnet $FePS_3$. *Phys Rev X* 2021; **11**: 011024.

168 Soriano D, Cardoso C, Fernández-Rossier J. Interplay between interlayer exchange and stacking in CrI_3 bilayers. *Solid State Commun* 2019; **299**: 113662.

169 Shao J, Liu Y, Zeng M, *et al.* Pressure-tuned intralayer exchange in superlattice-like $MnBi_2Te_4/(Bi_2Te_3)_n$ topological insulators. *Nano Lett* 2021; **21**: 5874–5880.

170 Bhoi D, Gouchi J, Hiraoka N, *et al.* Nearly room-temperature ferromagnetism in a pressure-induced correlated metallic state of the van der Waals insulator $CrGeTe_3$. *Phys Rev Lett* 2021; **127**: 217203.

171 Arneth J, Jonak M, Spachmann S, *et al.* Uniaxial pressure effects in the two-dimensional van der Waals ferromagnet CrI_3. *Phys Rev B* 2022; **105**: L060404.

172 Pawbake A, Pelini T, Delhomme A, *et al.* High-pressure tuning of magnon-polarons in the layered antiferromagnet $FePS_3$. *ACS Nano* 2022; **16**: 12656–12665.

173 Lv HY, Lu WJ, Luo X, *et al.* Strain- and carrier-tunable magnetic properties of a two-dimensional intrinsically

ferromagnetic semiconductor: $CoBr_2$ monolayer. *Phys Rev B* 2019; **99**: 134416.

174 Zhang X, Wang L, Su H, *et al.* Strain tunability of perpendicular magnetic anisotropy in van der Waals ferromagnets VI_3. *Nano Lett* 2022; **22**: 9891–9899.

175 Zhong J, Wang M, Liu T, *et al.* Strain-sensitive ferromagnetic two-dimensional Cr_2Te_3. *Nano Res* 2022; **15**: 1254–1259.

176 Cao Y, Fatemi V, Demir A, *et al.* Correlated insulator behaviour at half-filling in magic-angle graphene superlattices. *Nature* 2018; **556**: 80–84.

177 Cao Y, Fatemi V, Fang S, *et al.* Unconventional superconductivity in magic-angle graphene superlattices. *Nature* 2018; **556**: 43–50.

178 Xie H, Luo X, Ye G, *et al.* Twist engineering of the two-dimensional magnetism in double bilayer chromium triiodide homostructures. *Nat Phys* 2022; **18**: 30–36.

179 Baibich MN, Broto JM, Fert A, *et al.* Giant magnetoresistance of (001)Fe/(001)Cr magnetic superlattices. *Phys Rev Lett* 1988; **61**: 2472–2475.

180 Binasch G, Grünberg P, Saurenbach F, *et al.* Enhanced magnetoresistance in layered magnetic structures with antiferromagnetic interlayer exchange. *Phys Rev B* 1989; **39**: 4828–4830.

181 Fert A, Grünberg P, Barthélémy A, *et al.* Layered magnetic structures: Interlayer exchange coupling and giant magnetoresistance. *J Magn Magn Mater* 1995; **140-144**: 1–8.

182 Moodera JS, Kinder LR, Wong TM, *et al.* Large magnetoresistance at room temperature in ferromagnetic thin film tunnel junctions. *Phys Rev Lett* 1995; **74**: 3273–3276.

183 Miyazaki T, Tezuka N. Giant magnetic tunneling effect in $Fe/Al_2O_3/Fe$ junction. *J Magn Magn Mater* 1995; **139**: L231–L234.

184 Wang QH, Bedoya-Pinto A, Blei M, *et al.* The magnetic genome of two-dimensional van der Waals materials. *ACS Nano* 2022; **16**: 6960–7079.

185 Klein DR, MacNeill D, Lado JL, *et al.* Probing magnetism in 2D van der Waals crystalline insulators via electron tunneling. *Science* 2018; **360**: 1218–1222.

186 Kim HH, Yang B, Patel T, *et al.* One million percent tunnel magnetoresistance in a magnetic van der Waals heterostructure. *Nano Lett* 2018; **18**: 4885–4890.

187 Yan Z, Zhang R, Dong X, *et al.* Significant tunneling magnetoresistance and excellent spin filtering effect in CrI_3-based van der Waals magnetic tunnel junctions. *Phys Chem Chem Phys* 2020; **22**: 14773–14780.

188 Pan L, Huang L, Zhong M, *et al.* Large tunneling magnetoresistance in magnetic tunneling junctions based on two-dimensional CrX_3 (X = Br, I) monolayers. *Nanoscale* 2018; **10**: 22196–22202.

189 Song T, Tu MWY, Carnahan C, *et al.* Voltage control of a van der Waals spin-filter magnetic tunnel junction. *Nano Lett* 2019; **19**: 915–920.

190 Jiang S, Li L, Wang Z, *et al.* Spin tunnel field-effect transistors based on two-dimensional van der Waals heterostructures. *Nat Electron* 2019; **2**: 159–163.

191 Li X, Lü JT, Zhang J, *et al.* Spin-dependent transport in van der Waals magnetic tunnel junctions with Fe_3GeTe_2 electrodes. *Nano Lett* 2019; **19**: 5133–5139.

192 Lin ZZ, Chen X. Ultrathin scattering spin filter and magnetic tunnel junction implemented by ferromagnetic 2D van der Waals material. *Adv Electron Mater* 2020; **6**: 1900968.

193 Albarakati S, Tan C, Chen ZJ, *et al.* Antisymmetric magnetoresistance in van der Waals Fe_3GeTe_2/graphite/Fe_3GeTe_2 trilayer heterostructures. *Sci Adv* 2019; **5**: eaaw0409.

194 Lin H, Yan F, Hu C, *et al.* Spin-valve effect in $Fe_3GeTe_2/MoS_2/Fe_3GeTe_2$ van der Waals heterostructures. *ACS Appl Mater Interfaces* 2020; **12**: 43921–43926.

195 Johansen Ø, Risinggård V, Sudbø A, *et al.* Current control of magnetism in two-dimensional Fe_3GeTe_2. *Phys Rev Lett* 2019; **122**: 217203.

196 Miron IM, Garello K, Gaudin G, *et al.* Perpendicular switching of a single ferromagnetic layer induced by in-plane

current injection. *Nature* 2011; **476**: 189–193.

197 Kurebayashi H, Garcia JH, Khan S, *et al.* Magnetism, symmetry and spin transport in van der Waals layered systems. *Nat Rev Phys* 2022; **4**: 150–166.

198 Wang X, Tang J, Xia X, *et al.* Current-driven magnetization switching in a van der Waals ferromagnet Fe_3GeTe_2. *Sci Adv* 2019; **5**: eaaw8904.

199 Afanasiev D, Hortensius JR, Ivanov BA, *et al.* Ultrafast control of magnetic interactions via light-driven phonons. *Nat Mater* 2021; **20**: 607–611.

200 Disa AS, Nova TF, Cavalleri A. Engineering crystal structures with light. *Nat Phys* 2021; **17**: 1087–1092.

201 Železný J, Wadley P, Olejník K, *et al.* Spin transport and spin torque in antiferromagnetic devices. *Nat Phys* 2018; **14**: 220–228.

202 Gomonay O, Baltz V, Brataas A, *et al.* Antiferromagnetic spin textures and dynamics. *Nat Phys* 2018; **14**: 213–216.

203 Liu ZQ, Chen H, Wang JM, *et al.* Electrical switching of the topological anomalous Hall effect in a non-collinear antiferromagnet above room temperature. *Nat Electron* 2018; **1**: 172–177.